

Decomposing and Editing Predictions by Modeling Model Computation

Harshay Shah
harshay@mit.edu
MIT

Andrew Ilyas
ailyas@mit.edu
MIT

Aleksander Mądry
madry@mit.edu
MIT

Abstract

How does the internal computation of a machine learning model transform inputs into predictions? In this paper, we introduce a task called *component modeling* that aims to address this question. The goal of component modeling is to decompose an ML model’s prediction in terms of its *components*—simple functions (e.g., convolution filters, attention heads) that are the “building blocks” of model computation. We focus on a special case of this task, *component attribution*, where the goal is to estimate the counterfactual impact of individual components on a given prediction. We then present COAR, a scalable algorithm for estimating component attributions; we demonstrate its effectiveness across models, datasets, and modalities. Finally, we show that component attributions estimated with COAR directly enable model editing across five tasks, namely: fixing model errors, “forgetting” specific classes, boosting subpopulation robustness, localizing backdoor attacks, and improving robustness to typographic attacks. We provide code for COAR at <https://github.com/MadryLab/modelcomponents>.

1 Introduction

Despite their predictive power, large-scale machine learning (ML) models remain black boxes. In particular, the complex internal computation that these models perform to transform inputs into predictions makes it difficult to understand model behavior and, as a result, detect failure modes prior to deployment [BVP18; SCN+19; GJM+20].

In response to this difficulty, a line of work in ML interpretability aims to shed light on model computation by analyzing *model components*—intuitively “grouped” model parameters such as convolutional filters or attention heads. For example, feature visualization methods [SVZ13; ZF14; GKB+22] identify components in vision models that detect visual concepts such as curves [OCS+20a] and objects [BZS+20]. Representation-based probes [AB16] identify groups of components in language models that encode sentiment [RJS17], part-of-speech tags [BLZ18], and syntactic structure [HL19]. Finally, mechanistic interpretability analyses [WVC+22; NCL+23] uncover specific components that encode a model behavior of interest, e.g., “knowledge neurons” [DDH+21] and “induction heads” [OEN+22]. Broadly, these works leverage different tools to answer the question: *How do individual model components shape model behavior?*

In this work, we propose a new (and complementary) approach to studying this question. Our point of start is to rephrase the question, instead asking:

How do changes to model components collectively change individual model predictions?

We turn this rephrased question into a concrete task called component modeling. In this task, the goal is to build an interpretable *counterfactual estimator* of how a model’s output would change in

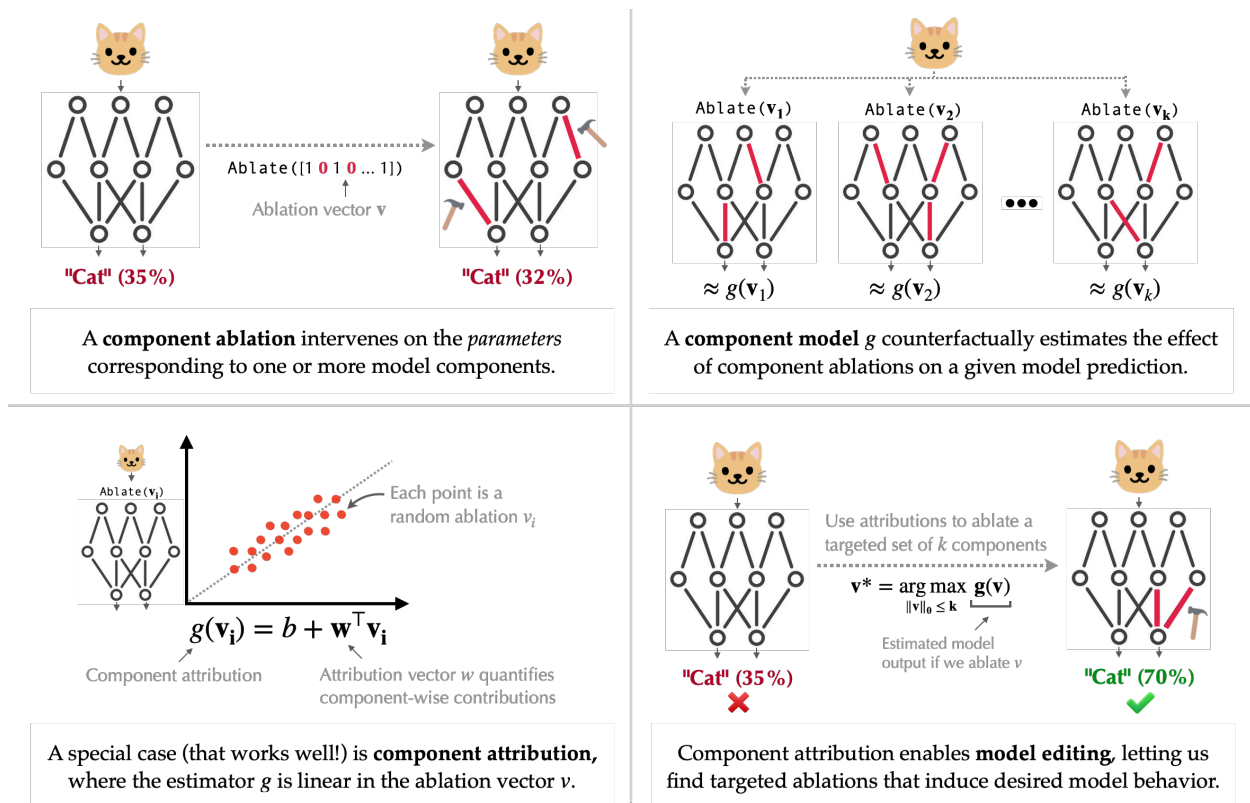


Figure 1: A summary of the component modeling framework.

response to interventions made to its components. In the rest of the paper, we present a general approach to building such estimators, which turn out to be highly predictive in large-scale settings. Beyond shedding light on how model components collectively contribute to a given prediction, these estimators enable effective model editing, allowing us to design targeted interventions that induce certain desirable model predictions.

Roadmap & contributions. The main contribution of our work is a framework for decomposing model predictions in terms of model components, which we show has direct applications to model editing. Figure 1 summarizes these contributions. Specifically, in this paper we:

1. **Introduce the component modeling framework:** We formalize our goal of understanding how model components shape ML predictions as a concrete task called *component modeling* (Definition 1). The objective of this task is to learn a counterfactual estimator, or *component model*, that accurately predicts the effect of ablating a subset of model components on a given model prediction (Equation 1). Intuitively, this task operationalizes the idea that if we can “understand” how model components shape a prediction, we should also be able to estimate how the prediction would change if we were to ablate a subset of components.
2. **Instantiate the framework via component attribution:** We focus our attention on a special “linear” case of component modeling called *component attribution*, where we assign a score to each component, and estimate the counterfactual effect of ablating a set of components as the sum of their corresponding scores (Definition 2). Component attributions allow us to

directly read off the “contribution” of every component to a prediction, abstracting away the complexity of the model’s internal computation.

3. **Propose an algorithm for efficient component attribution:** We develop COAR (component attribution via regression), a scalable way to estimate component attributions (Section 3). Through experiments on both image classifiers and language models, we show that COAR yields component attributions that can accurately predict how model predictions change in response to component-level ablations (Section 4).
4. **Demonstrate that component attributions enable model editing:** Component attributions from COAR directly enable edits to large-scale classifiers without additional training (Section 5). Specifically, we propose an editing procedure (COAR-EDIT) that designs targeted ablations by using COAR attributions as a counterfactual estimator—given an objective, COAR-EDIT finds ablations for which estimated model outputs perform well. We stress-test COAR-EDIT through five editing tasks: fixing model errors (§5.1), selectively “forgetting” an entire class (§5.2), boosting subpopulation robustness (§5.3), localizing backdoor attacks (§5.4), and mitigating typographic attacks (§5.5).

Paper organization. We begin by formalizing the component modeling task and its special case, component attribution, in Section 2. We then describe our method, COAR, for estimating component attributions in Section 3, and demonstrate its effectiveness on large-scale models in Section 4. Finally, we stress-test the practical utility of COAR attributions for model editing in Section 5.

2 Setup and Problem Statement

Consider a typical supervised learning setup. We have a set S of input-label pairs (or *examples*) $z_i = (x_i, y_i)$, and a trained model M that maps inputs x to predicted labels $M(x)$. We define the *model output function* $f_M(z) \in \mathbb{R}$ as any statistic that quantifies the correctness of model M on the example z . For instance, the model output $f_M(z)$ can be the cross-entropy loss in a classification task, or the squared loss in a regression task.

In this work, we will think of the model M not as a black box, but instead as the output of a *computation graph* G_M [Bau74]. Each parameterized node of this graph—which we call a *component*—is a function mapping its incoming edges to an outgoing edge. For example, a d -dimensional linear model M naturally admits a computation graph G_M with d components—one component $C_i(z) = w_i \cdot z$ for each parameter w_i —followed by a summation that combines the components into an output.

For more complex models, there are often multiple valid computation graphs G_M we could consider. For example, if M is a Transformer [VSP+17], the components might be multi-head attention blocks, individual attention heads, or even individual parameters. In general, the component set depends on the model architecture *and* the level of granularity that we wish to study.

Component modeling. Our goal in this work is to understand the behavior of the model M in terms of its components. By viewing the model M as a computation graph G_M over a set of components C , we can restate our goal as follows:

Given a model M and example z , how do individual components $c \in C$ combine to yield the model output $f_M(z)$?

Of course, there is a trivial answer to this question: the components $c \in C$ combine through the very computation graph used to define C . This answer is correct but not satisfying, as it does not get us closer to our conceptual goal of understanding model behavior in terms of components.

What we are truly after is a *simple, interpretable* function capturing how components in C impact $f_M(z)$. To make this more precise, we define the *component counterfactual function* $f_M(z, C')$ as

$$f_M(z, C') := \text{model output } f_M(z) \text{ on example } z \text{ after ablating components } C' \subseteq C, \quad (1)$$

where “ablating” here corresponds to any intervention that overrides or patches the parameters corresponding to components $c \in C'$ (e.g., by setting them to zero [OEN+22] or by adding random noise [MBA+22]).

Equation (1) allows us to operationalize our goal as a *counterfactual estimation* task. In this task, we want to estimate component counterfactuals $f_M(z, C')$ using a much simpler function, which we call a component model.

Definition 1 (Component modeling). *Fix a model M with computation graph G_M , component set $C = \{c_1, \dots, c_N\}$, and model output function f_M . For any subset of model components $C' \subseteq C$, let $\mathbf{0}_{C'}$ be the corresponding ablation vector of C' , defined as a N -dimensional vector where*

$$(\mathbf{0}_{C'})_i = \begin{cases} 0 & \text{if } c_i \in C' \\ 1 & \text{otherwise.} \end{cases}$$

Given an example z , a component model for z is a function $g^{(z)} : \{0, 1\}^N \rightarrow \mathbb{R}$ that maps ablation vectors of subsets C' to estimates of the counterfactual $f_M(z, C')$.

In other words, the high-level goal of component modeling is to build an estimator that can directly answer counterfactual questions like “*what would happen to my classifier’s prediction on a given image if I ablated a specific set of components $C' \subseteq C$?*” without having to intervene on the computation graph G_M and ablate components in C' .

Component attribution. In this work, we consider a subcase of component modeling—which we call *component attribution*—where the function $g^{(z)}$ is *linear* in its input. That is, a component attribution for example z assigns a score $w_i^{(z)}$ to each component $c_i \in C$, and predicts the effect of ablating $C' \subset C$ as the sum of the scores corresponding to components in $C \setminus C'$.

Definition 2 (Component attribution). *Fix a model M with output function f_M and component set $C = \{c_1, \dots, c_N\}$. A component attribution for example z is a set of parameters $\theta^{(z)} := \{w_1^{(z)}, \dots, w_N^{(z)}, b^{(z)}\}$ which parameterize a linear component model, i.e., a function $g^{(z)}$ such that*

$$f_M(z; C') \approx g^{(z)}(\mathbf{0}_{C'}) := \mathbf{0}_{C'}^\top \mathbf{w}^{(z)} + b^{(z)}$$

Component attribution satisfies our goal of finding a simple, interpretable account of how model components combine to form predictions. In particular, a component attribution for example z decomposes a model’s output on z into the contributions $w_i^{(z)}$ of each individual component c_i .

Remark 1 (Linearity and misspecification). *Modern ML models comprise complex computation graphs with highly non-linear interactions among model components. For such models, it is unclear a priori why the effect of ablating components on model outputs (i.e., component counterfactuals (1)) should be well-approximated by linear component attributions (2), which sum fixed additive effects of individual components. Still, despite this evident misspecification, our results on large-scale vision and language models in Section 4 show that component attributions can accurately predict component counterfactuals.*

3 Component attribution with COAR

In Section 2, we formalized our high-level goal of understanding how models internally process examples into a counterfactual estimation task called *component modeling* (Definition 1), of which we study a special (linear) case called *component attribution* (Definition 2). Now, we show how to estimate component attributions $\theta^{(z)}$ by casting the counterfactual estimation task as a regression problem. Specifically, we now describe COAR (component attribution via regression), a general component attribution method for models ranging from random forests to deep neural networks.

Approach. Consider a fixed model output $f_M(\cdot)$ of interest, and a corresponding computation graph G_M that encodes the model components C at the desired level of granularity. Additionally, we fix an *ablation method*, i.e., a procedure for “overriding” or patching any given subset $C' \subset C$ of the model components in the computation graph G_M .

Our method COAR takes in an example z and outputs a corresponding component attribution vector $\theta^{(z)} \in \mathbb{R}^{|C|+1}$ (Definition 2). To do so, COAR casts the task of predicting component counterfactuals as a *supervised learning* problem, which we solve in two steps:

1. **Construct a component dataset.** We construct a dataset $D^{(z)}$ of component counterfactuals for the example z . Each “datapoint” in $D^{(z)}$ consists of a component subset $C_i \subseteq C$ and its corresponding counterfactual $f_M(z, C_i)$ (see (1))—we evaluate the latter by simply ablating the components in C_i and evaluating the model on example z .

In this work, we choose the component subsets C_i to be random α_{train} -fraction subsets of the component set C , for a ablation fraction hyperparameter $\alpha_{\text{train}} > 0$.¹ The output of this step is a *component dataset*

$$D^{(z)} := \{(C_1, f_M(z, C_1)), \dots, (C_m, f_M(z, C_m))\}, \quad (2)$$

where $C_i \sim \text{Uniform}(\{C' \subset C : |C'| = \alpha_{\text{train}}|C|\})$. We study the effect of varying the ablation fraction α on COAR in Appendix E.1.

2. **Fit a linear estimator.** We then use the dataset $D^{(z)}$ to fit component attribution parameters $\theta^{(z)}$ for each example z (see Definition 2). More specifically, for each example z , we minimize the squared loss between the component counterfactuals from Step 1 and their corresponding attribution-based predictions by solving the following *linear regression* problem:

$$\theta^{(z)} := \arg \min_{b \in \mathbb{R}, w \in \mathbb{R}^{|C|}} \sum_{(C_i, f_M(z, C_i)) \in D^{(z)}} \left(b + \mathbf{0}_{C_i}^\top w - f_M(z, C_i) \right)^2, \quad (3)$$

where again $\mathbf{0}_{C_i}$ is the ablation vector of C_i (Definition 1). Our component model is then

$$g^{(z)}(\mathbf{0}_{C'}) := \mathbf{0}_{C'}^\top w^{(z)} + b^{(z)}. \quad (4)$$

We provide pseudocode for COAR in Appendix A.1. As we discussed in Section 2, the resulting component attribution $\theta^{(z)} := (w^{(z)}, b^{(z)})$ is interpretable in that the coefficient $w_j^{(z)}$ estimates how the model output on example z would change if we were to ablate component c_j . We can thus view this coefficient as the (estimated) additive contribution of component c_j to the model output.

¹We opt for this random α -fraction sampling method for simplicity—it may be possible to make COAR more statistically efficient by choosing the subsets C_i more carefully.

The above two-step approach is simple and highly scalable—we can construct the dataset $D^{(z)}$ with just forward passes on the given model to compute component counterfactuals, and optimize the linear regression problem (eq. 3) with off-the-shelf GPU-based solvers—see Appendix A.4 for details. This enables us to apply COAR on large-scale models (e.g., ViT [DBK+21]) and datasets (e.g., ImageNet [DDS+09]), as shown in the next section.

Instantiating COAR for classifiers. Our method COAR is *general* in that we can use it to study any machine learning model M that has a corresponding output function f_M and computation graph G_M . In this work, we primarily use COAR to analyze models trained on classification tasks. Although the computation graph G_M will vary based on the specific model architecture we are studying, across all models we use the standard *correct-class margin* [IPE+22] as the model output f_M , i.e.,

$$f_M(z) := (\text{logit for correct class}) - (\text{highest logit for incorrect class}). \quad (5)$$

a quantity whose sign indicates the correctness of model M on the example z . For the latter, we choose to ablate component subsets $C' \subset S$ by simply setting the parameters of the components in C' to zero [WVC+22; OEN+22]. We use COAR with alternative model output functions and ablation methods in Appendix E.3 and Appendix E.2 respectively.

Remark 2 (Ablation is not removal). *As noted in prior work [CGG+22], ablation methods (e.g., setting weights or activations to zero) do not “remove” model components from the computation graph. Instead, such ablations shift the activations off-distribution in a systematic way—the goal of component attribution (Definition 2) is to predict the change in model outputs induced by this shift. We use zero-ablation as our ablation method because it is a common choice in the literature [OEN+22; WVC+22]. In Appendix E.2, we show that COAR can estimate component attributions with alternative ablation methods as well.*

4 Does COAR learn accurate component attributions?

We now evaluate whether COAR-estimated attributions accurately predict component counterfactuals (as in (1)) for deep neural networks trained on image classification and language modeling.

Datasets, models, and components. We apply COAR to compute component attributions in three different setups:

- **Setup A:** A ResNet-18 [HZR+15] trained on the CIFAR-10 dataset [Kri09], with a computation graph G_A comprising $|C| = 2,306$ components. Specifically, each model component $c_i \in C$ corresponds to a convolutional filter in the model, and ablating a set of components $C' \subset C$ means setting all the weights in the corresponding filters to zero.
- **Setup B:** A ResNet-50 trained on the ImageNet dataset [DDS+09], with a computation graph G_B comprising $|C| = 22,720$ components. Again, each component here corresponds to a convolutional filter in one of the 49 convolution layers of the ResNet-50.
- **Setup C:** A Vision Transformer (ViT-B/16) [DBK+21] trained on ImageNet, whose computation graph G_C comprises 82,944 components. Each component here corresponds to a row of a weight matrix in one of 12 transformer blocks of the ViT, and ablating a set of components means setting the corresponding rows to zero.

We provide additional details on the models and datasets in Appendix A.2.

Applying COAR. We use COAR to obtain component attributions (one for each test example) in each setup. Specifically, for a given model, we first construct a component dataset $D^{(z)}$ for each example z (as in Step 1 of Section 3) by randomly ablating α_{train} fraction of all components and evaluating the resulting correct-class margin (5) on z , where $\alpha_{\text{train}} = \{10\%, 5\%, 5\%\}$ for setup $\{A, B, C\}$ above. We repeat this m times, yielding a component dataset $D^{(z)}$ of size m for each example z —we use $m = \{50000, 100000, 200000\}$ for setup $\{A, B, C\}$ above. We then run linear regressions on the resulting datasets (as in Step 2 of Section 3) to yield the final component attributions. We defer implementation details to Appendix A.4 and study the effect of the dataset size m and ablation fraction α_{train} on the resulting attributions in Appendices C.4 and C.5.

Evaluation metric. We evaluate component attributions based on their ability to estimate *unseen* component counterfactuals (1), i.e., the result of ablating component subsets C' not observed at training time. Specifically, we sample a new collection of k component subsets

$$D_{\text{test}}^{(z)} := \{C'_1, C'_2, \dots, C'_k\}, \quad \text{where} \quad C'_i \sim \text{Unif}(\{C' \subset C : |C'| = \alpha_{\text{test}}|C|\}),$$

where $0 < \alpha_{\text{test}} < 1$ is the ablation fraction used at evaluation time. Varying α_{test} allows us to evaluate attributions on in-distribution ($\alpha_{\text{test}} = \alpha_{\text{train}}$) and out-of-distribution ($\alpha_{\text{test}} \neq \alpha_{\text{train}}$) component counterfactuals.

To quantify the predictiveness of component attributions, we use $D_{\text{test}}^{(z)}$ to measure the Pearson correlation between component counterfactuals $f_M(z, C'_i)$ and their corresponding attribution-based estimates $g^{(z)}(\mathbf{0}_{C'_i})$ (eq. 4.), i.e.,

$$\rho(z) := \text{Pearson-}\rho\left(\underbrace{\{f_M(z, C'_1), \dots, f_M(z, C'_k)\}}_{\text{ground-truth counterfactuals}}, \underbrace{\{g^{(z)}(\mathbf{0}_{C'_1}), \dots, g^{(z)}(\mathbf{0}_{C'_k})\}}_{\text{attribution-based estimates}}\right). \quad (6)$$

Baselines. We use the evaluation metric described above (Equation 6) to compare COAR attributions with four baselines, two adapted from related work and two natural baselines. We defer implementation details to Appendix A.3.

- **Adapted baselines (NC, II):** We adapt **neuron conductance (NC)** [DSY18] and **internal influence (II)** [LSD+18] to the component attribution setting. Both methods use integrated gradients [STY17] (an input-space feature attribution method) to compute importance scores for each component c_i . To compare these methods to COAR, we apply NC and II to model outputs on example z , and interpret the resulting scores as the attribution coefficients $w_i^{(z)}$.
- **Specialized baselines (L00, GP):** We also consider two other baselines. First, **leave-one-out (L00)** ablates individual components c_i and estimates the corresponding coefficient based on the effect of the ablation, setting $w_i^{(z)} = f_M(z, \{c_i\}) - f_M(z, \emptyset)$. We also consider **gradient-times-parameter (GP)**, which approximates the leave-one-out effect of each component using a first-order Taylor approximation, setting $w_i^{(z)} = \nabla_{c_i} f_M(z, \emptyset) \cdot \delta_{c_i}$, where δ_{c_i} is the parameter-space change in c_i induced by the ablation method of choice.

Remark 3 (Relation between baselines and patching). *Readers familiar with the field of mechanistic interpretability may observe that the leave-one-out (L00) baseline resembles activation patching [VGB+20; MBA+22; ZN23] and the gradient-times-parameter (GP) baseline resembles attribution patching [SRC23; KLS+24]. Indeed, activation patching ablates individual activations to estimate their effect, and attribution patching considers a first-order gradient-based approximation. The key difference is that the ablations we consider are in parameter space rather than activation space, and that we study a different model output.*

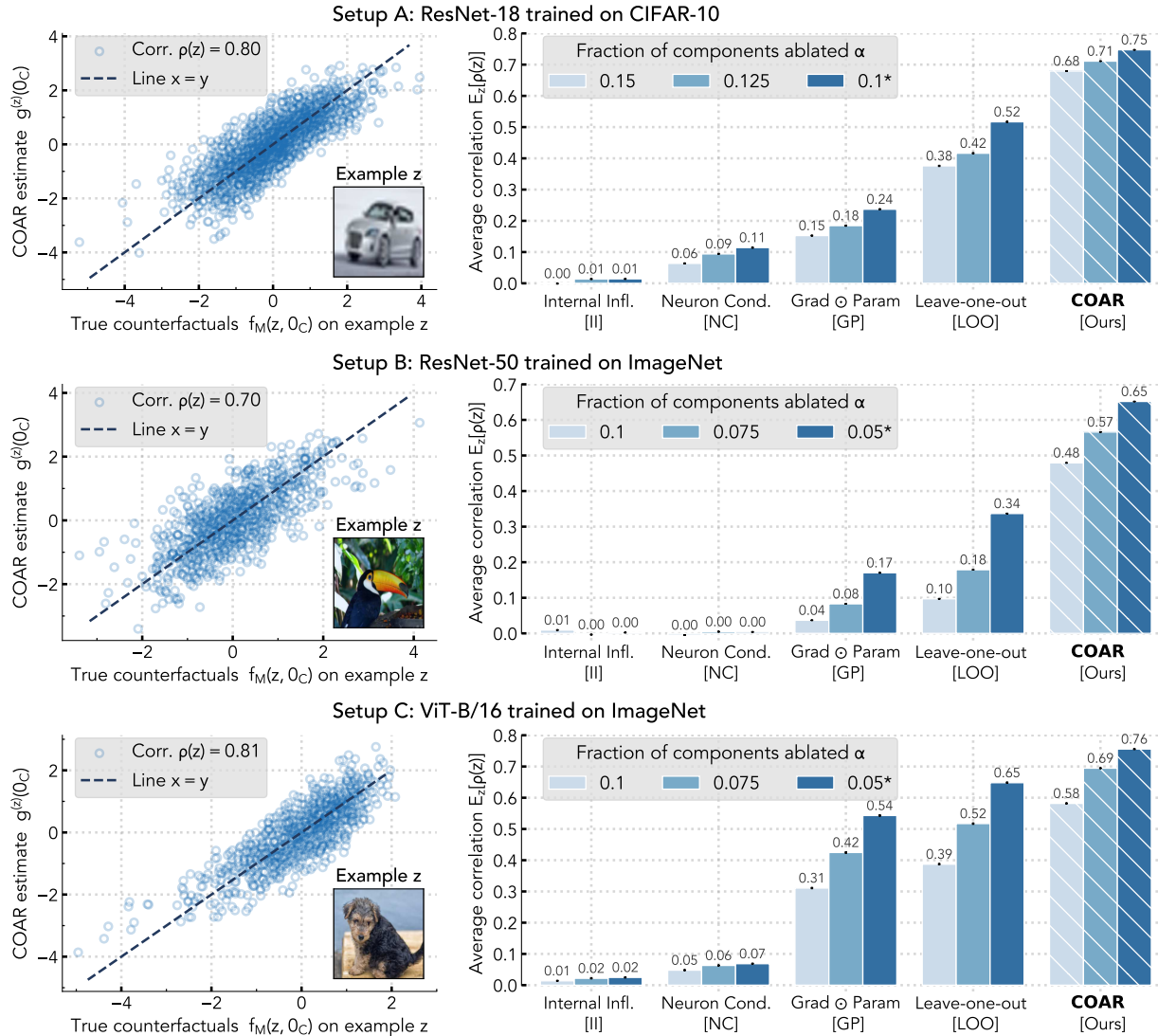


Figure 2: Evaluating COAR attributions. We evaluate whether component attributions computed using our procedure COAR accurately predict component counterfactuals (1). We compare COAR to four baselines (described in Section 4) on three image classification setups (one per row). The subfigures on the left each focus on a single example z (visualized in the bottom-right corner of each plot), and show that for each setup, the ground-truth component counterfactuals $f_M(z, \cdot)$ (x -axis) and attribution-based estimates $g^{(z)}(\cdot)$ (y -axis) exhibit high correlation $\rho(z)$. On the right, we observe that COAR attributions exhibit high average correlation $\mathbb{E}_z[\rho(z)]$ over test examples, outperforming all baselines in each task and for all ablation fractions α_{test} . The asterisk (*) in each legend denotes α_{train} , the ablation fraction used to fit the component attributions.

4.1 Results

We now use the setup described above to test whether COAR learns accurate component attributions for setups $\{A, B, C\}$. For each task, we first use COAR to estimate a component attribution for every example z in the corresponding test set. We then evaluate these component attributions using the correlation metric $\rho(z)$ defined in Equation 6. Figure 2 depicts our results.

Example-level analysis. On the left side of each row in Figure 2, we focus on an *individual test example* z from each task. For each example z , we ablate random component subsets $C' \subset C$ of size $\alpha_{\text{test}} \cdot |C|$ (for $\alpha_{\text{test}} = \alpha_{\text{train}}$) from the model and estimate the correlation $\rho(z)$ from Equation 6. Across all three tasks, we observe that COAR learns accurate component attributions for the selected test examples. In Appendix C.6, we provide additional (randomly selected) example-specific correlation plots, as well as analogous plots for all baselines described above.

Aggregate analysis. The right side of each row in Figure 2 plots the *average* correlation between the ground-truth counterfactuals and attribution-based estimates over test examples, i.e., $\mathbb{E}_z[\rho(z)]$. We also analyze the effect of ablation fraction α_{test} on the average correlation, finding that:

- (a) COAR outperforms baselines by a large margin across datasets, models, and ablation fractions α_{test} . For example, when ablating $\alpha_{\text{test}} = 5\%$ of components in the ImageNet ResNet50 (setup B), attribution-based estimates using COAR and the best-performing baseline (L00) exhibit 0.65 and 0.34 correlation with ground-truth counterfactuals, respectively. Additionally, the adapted baselines, NC and II, exhibit low correlation with the ground-truth counterfactuals in all three setups.
- (b) The correlation between ground-truth counterfactuals and attribution-based estimates decays gracefully on larger out-of-distribution component subsets, i.e., as α_{test} increases. For example, increasing α_{test} from 10% (equal to α_{train}) to 12.5% and 15% on CIFAR-10 (setup A) only decreases the average correlation of COAR-based estimates from 0.74 to 0.70 and 0.68 respectively.

Applying COAR to language models. Although we focus on vision models in this work, our attribution method COAR is general and modality-agnostic. In Appendix B, we show that COAR, without any modification, yields predictive component attributions for language models as well. First, we apply COAR to GPT-2 [RWC+19] evaluated on the next-token prediction task using the TinyStories dataset [EL23] (§B.1). Then, we turn to the zero-shot classification setting and apply COAR to Phi-2 [LBE+23] evaluated on the BoolQ question-answering task [CLC+19] (§B.2).

Additional analysis. In Appendix C, we show that COAR attributions are predictive for out-of-distribution inputs (§C.1), additional architectures (§C.2), additional tasks (§C.3), and different train-time ablation fractions (§C.4). We also show that COAR outperform baselines when trained with $2\text{-}5\times$ fewer samples in Appendix C.5, and provide qualitative analysis in Appendix C.7.

5 Do COAR attributions enable model editing?

In the last section, we showed that COAR attributions accurately predict how model outputs change in response to component-level interventions. We now evaluate the practical utility of COAR by applying it to the problem of *model editing*. That is, we ask:

Is ablating model components identified via COAR attributions an effective way to edit models?

To answer this question, we first define model editing in our context and provide a simple method, COAR-EDIT, for translating component attributions into model edits. We apply this approach to edit model behavior on individual examples (§5.1), classes (§5.2), subpopulations (§5.3), and concepts (§5.4, §5.5). Our findings indicate that COAR *directly* enables model editing.

Problem setup. Consider a machine learning model M , a target distribution over examples \mathcal{D}_T , and a reference distribution \mathcal{D}_R . A *model edit* on M is an intervention that aims to modify performance on the target examples $z \sim \mathcal{D}_T$ in a specific way, while leaving behavior on reference examples $z \sim \mathcal{D}_R$ unchanged. In its most general version, model editing can involve additional training (e.g., constrained fine-tuning [ZRZ+20] or rank-one parameter updates [BLW+20]), targeted modifications to model parameters (e.g., weight pruning [DSH+21] or hypernetworks [MLB+21]), or even architectural modifications (e.g., adaptors [HSP+22] or adding neurons [HSZ+23]).

Since our goal is to study model predictions in terms of model components, we restrict model edits to *ablation-based* interventions in this work. That is, we only consider interventions whose output can be expressed as component counterfactuals (see Equation 1). The goal of an editing method, then, is to identify a subset of model components whose ablation changes performance on a given target set of examples S_T , without impacting model behavior on a reference set of examples S_R . Definition 3 turns this intuition into a precise definition of the ablation-based model editing problem.

Definition 3 (Editing models by ablating components). *Consider a model M with computation graph G_M , component set $C = \{c_1, \dots, c_N\}$, and model output function f_M . Let \mathcal{D}_T and \mathcal{D}_R denote target and reference distributions over examples, respectively. An (ϵ, δ) -effective model edit for \mathcal{D}_R and \mathcal{D}_T is an intervention that ablates a subset of components $C_{edit} \in 2^C$ such that*

$$\underbrace{\mathbb{E}_{\mathcal{D}_R}[|f_M(z, C_{edit}) - f_M(z, \emptyset)|]}_{\text{Effect of edit on reference examples is small}} \leq \epsilon \quad \text{and} \quad \underbrace{\mathbb{E}_{\mathcal{D}_T}[|f_M(z, C_{edit}) - f_M(z, \emptyset)|]}_{\text{Effect of edit on target examples is large}} \geq \delta, \quad (7)$$

where $f_M(z, C)$ denotes the component counterfactual function (1), i.e., model output function f_M evaluated on example z after ablating components C .

As per Definition 3, each component subset $C' \subset 2^C$ defines a potential model edit. That is, effectively editing the model (as in (7)) requires identifying a subset C' that, when ablated, significantly changes model outputs on the target distribution but not on the reference distribution. A naive approach to this task would thus require searching over the (combinatorial) space of all possible component subsets. Is there a better way?

An attribution-based approach to model editing. In this section, our goal is to show that an effective component attribution method (such as COAR) can directly serve as a guide for identifying effective model edits. Key to this utility is a fundamental connection between the attribution problem and the editing problem. In particular, the former answers questions of the form, “*how would the model outputs change if we were to ablate a subset of components?*” while the latter inverts this question to ask “*which components, when ablated, would change model outputs in a specific way?*” By identifying the model components that are most “important” to the desired model outputs, an attribution method can thus identify a subset of model components to target through ablation-based editing (see Definition 3).

To make this concrete, we propose COAR-EDIT, a simple three-step editing approach based on COAR attributions. Specifically, given a model M with a set of model components C , a set of target examples S_T sampled from \mathcal{D}_T , and a set of reference examples S_R sampled from \mathcal{D}_R , COAR-EDIT identifies a model edit (7) in three steps:

1. Estimate COAR attributions $\theta^{(z)} := (\mathbf{w}^{(z)}, b^{(z)})$ where $\mathbf{w}^{(z)} \in \mathbb{R}^{|C|}$ and $b^{(z)} \in \mathbb{R}$ for every target and reference example $z \in S_T \cup S_R$.

- For each model component $c_i \in C$, use a simple t -test in order to quantify the “importance” of component c_i to set of target examples S_T relative to the set of reference examples S_R :

$$\tau(c_i) := \frac{\mu_i(S_T) - \mu_i(S_R)}{\sqrt{\frac{\sigma_i^2(S_T)}{|S_T|} + \frac{\sigma_i^2(S_R)}{|S_R|}}}, \quad \text{where} \quad \begin{cases} \mu_i(S) = \frac{1}{|S|} \sum_{z \in S} w_i^{(z)} \\ \sigma_i^2(S) = \frac{1}{|S|} \sum_{z \in S} (w_i^{(z)} - \mu(S))^2. \end{cases} \quad (8)$$

- To increase model outputs on target examples, ablate a set of components C_{edit} that contains the k most negative scores τ_i , i.e., set

$$C_{\text{edit}} = \arg \text{bottom-}k(\{\tau(c_i) : c_i \in C\}), \quad (9)$$

where the number of ablated components k is a hyperparameter which one can set, e.g., by cross-validation. Similarly, if the goal is to *decrease* model outputs on S_T , we replace bottom- k with top- k in (9).

To make sense of the approach above, note that for every component c_i and a set of examples S , $\mu(S)$ in Equation 8 leverages attributions to directly estimate $\mu_i(S)$, the average effect of ablating c_i on model predictions for samples in set S . Similarly, the term $\sigma_i^2(S)$ captures the variation (across examples) of this effect. As a result, the score $\tau(c_i)$ in Equation 8 exactly corresponds to the two-sample t -test statistic, with a null hypothesis that the component c_i has an equal average effect on the target distribution \mathcal{D}_T and the reference distribution \mathcal{D}_R . We then use these scores $\{\tau(c_i) : c_i \in C\}$ in Equation 9 in order to identify components that, when ablated, would change outputs on target examples the most relative to the change in the outputs of reference examples.

Remark 4 (Ablation-based edits). *Our restriction of model edits to ablations of component subsets in COAR-EDIT is a significant one. In particular, simply ablating model components is likely not the most effective way of editing a model. Our goal in this section, however, is not to propose a state-of-the-art model editing method, but rather to answer two questions. First, we want to assess the practical utility of COAR for informing model edits. Second, we want to shed light on whether large-scale models are amenable to zeroth-order editing, i.e., without gradient information. Leveraging COAR attributions in conjunction with editing techniques based on fine-tuning in order to make finer-grained model edits is an interesting direction for future work.*

Next, we use COAR-EDIT to edit large-scale models trained on classification tasks, where we use correct-class margin (5) as the model output function. Specifically, we conduct five experiments to evaluate the effectiveness of COAR-EDIT in editing model behavior using only a few examples and without requiring additional training.

- In Section 5.1, we correct individual model errors without impacting overall performance;
- In Section 5.2, we selectively “forget” a specific class while preserving model performance on other classes;
- In Section 5.3, we start with a model that performs disparately across a set of subpopulations, and edit the model to improve its accuracy on underperforming subpopulations;
- In Section 5.4, we localize (known) backdoor attacks and mitigate them by ablating a small number of components;
- In Section 5.5, we edit CLIP classifiers to be more robust to typographic attacks.

For all experiments, we provide additional details and analyses in Appendix D.

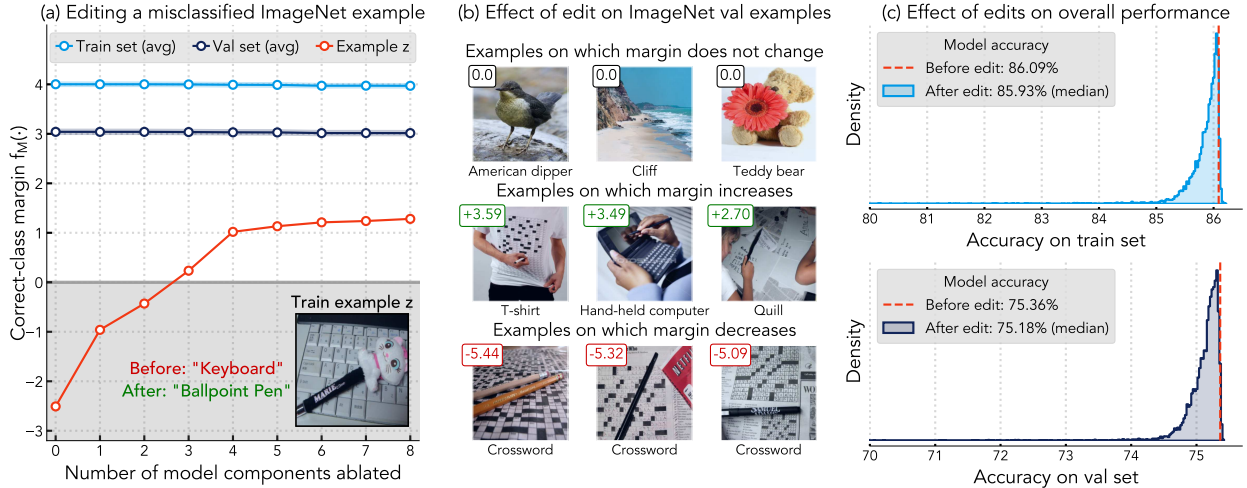


Figure 3: **Editing individual model predictions with COAR-EDIT.** We edit a ResNet50 model to correct a misclassified ImageNet example z shown on the left. Specifically, ablating a few components via COAR-EDIT (see (9)) increases the correct-class margin (5) on example z (red) without changing the average margin on the train set (light blue) or validation set (dark blue). In the center panel, we observe that the examples on which model outputs change the least (top row) due to the edit are visually dissimilar to example z as well as examples on which model outputs change most positively (middle row) and negatively (bottom row). On the right, we find that individually performing model edits to correct every misclassified example in the validation set incurs a median accuracy drop of at most 0.2% on the train set (top row) and validation set (bottom row).

5.1 Editing individual model predictions

In this section, we test whether COAR-EDIT can modify individual predictions of an ImageNet ResNet50 classifier (Setup B in Section 4) without impacting its overall performance. Specifically, we study the case where the target distribution \mathcal{D}_T is a singleton example on which we want to improve performance. An effective model edit in this context (Definition 3) would increase the model’s margin (5) on z to be greater than zero without affecting aggregate model performance.

Results. We apply COAR-EDIT to edit individual misclassified examples z , setting $S_T = \{z\}$ and S_R to be a small set of random samples from the ImageNet dataset. We present our findings in Figure 3. Figure 3a illustrates a single such edit, where we correct the model’s prediction on a specific ImageNet example from “keyboard” to “ballpoint pen” by ablating $k = 3$ components (0.01% of all components). Specifically, increasing the number of ablated components k consistently improves the correct-class margin on target example z (red) without changing the average margin over the training set (light blue) or validation set (dark blue). Figure 3b then visualizes (again, for the specific example being edited in Figure 3a) the examples on which model outputs changes most (and least) drastically. A qualitative inspection here suggests that examples with unchanged margins are dissimilar to z (first row), whereas examples that are most positively (second row) or negatively (third row) impacted share similar visual features with z , e.g., pen-like objects. Finally, Figure 3c shows that we can individually fix *every* misclassification in the ImageNet validation set while incurring a median accuracy drop of 0.2% on the training set (top row) and validation set (bottom row). We defer experiment details and additional results to Appendix D.1.

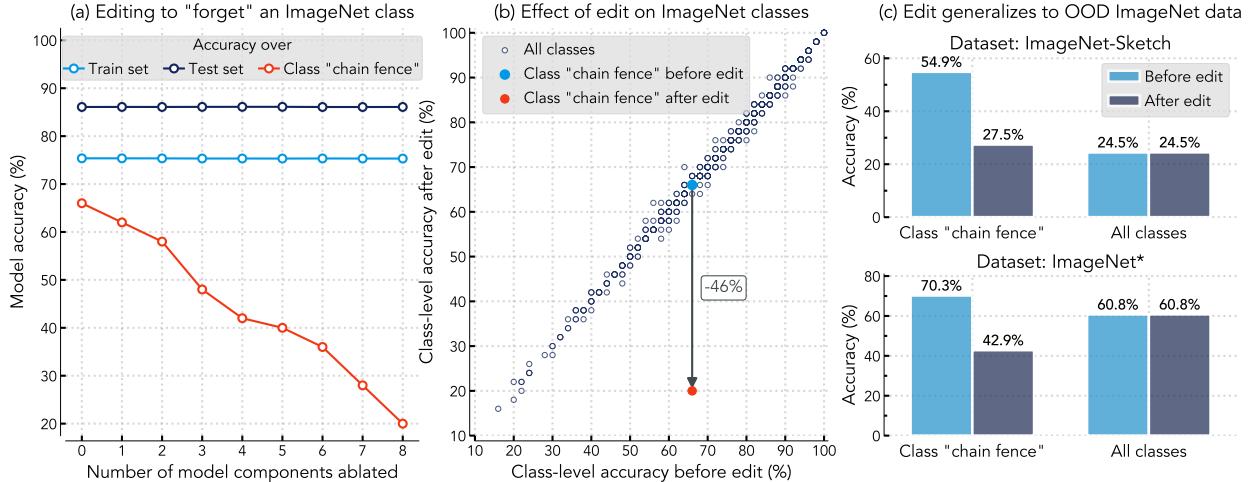


Figure 4: **“Forgetting” a class with COAR-EDIT.** We edit an ImageNet-trained ResNet-50 (Setup B from Section 4) to selectively degrade performance on the “chain-link fence” class. On the left, we observe that increasing the number of components k ablated via COAR-EDIT decreases model accuracy on the “chain-link fence” class (red) while preserving overall accuracy on the train and validation set. In the center panel, we compare class-wise accuracies before and after performing the model edit and observe a significant accuracy drop on the “chain-link fence” class but not on other classes. On the right, we find that the edit transfers to distribution-shifted versions of ImageNet (ImageNet-Sketch [WGX+19] and ImageNet* [VJE+23]) as targeted, i.e., degrading performance on the “chain-link fence” class without changing average performance.

5.2 “Forgetting” a class

We now consider “selective forgetting” problem [WYS+23], where the goal is to impair model performance on (only) a specific set of examples. In this experiment, we edit the same ImageNet ResNet-50 model (Setup B) as in Section 5.1, with the goal of forgetting the entire “chain-link fence” class. Like before, we use our editing approach COAR-EDIT (see (8) and (9)) to identify components that, when ablated, decrease the model’s correct-class margin on examples from the “chain-link fence” class, but not on reference examples from other classes.

Results. Figure 4 summarizes our findings. In Figure 4a, we show that ablating just eight (out of 22,720) model components degrades accuracy on the “chain fence” class from 66% to 20% while preserving overall accuracy on the train and validation set. Then, in Figure 4b, a comparison of class-wise accuracies before and after the edit shows that our approach specifically targets the “chain fence” class without impacting performance on any other class. Finally, in Figure 4c, we evaluate model performance on ImageNet-Sketch [WGX+19] (top) and ImageNet* [VJE+23] (bottom) datasets to show that the our edit is robust to distribution shifts in both the target and reference distribution. Through additional experiments in Appendix D.2, we highlight that (a) our approach is sample-efficient, not needing many samples from the target and reference distributions to find effective edits; and (b) our findings are robust to the choice of class to forget.

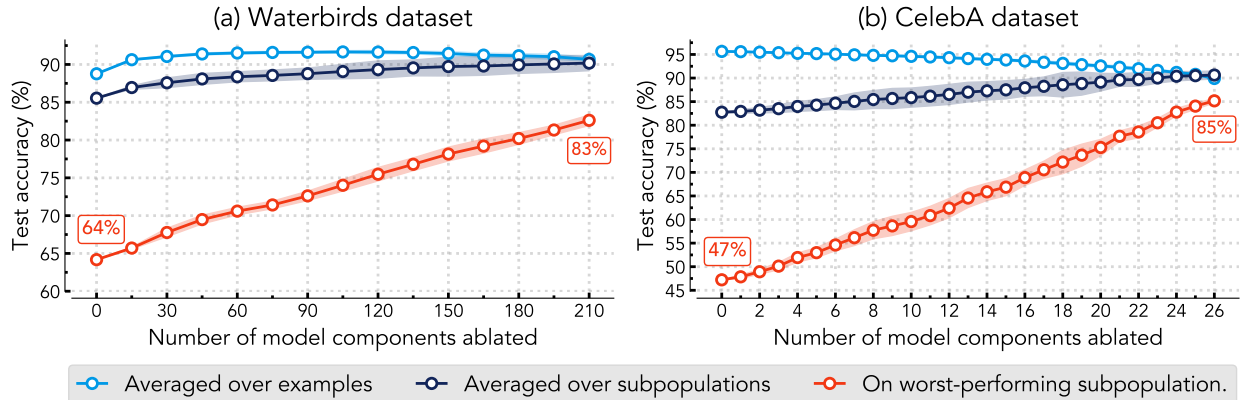


Figure 5: **Improving subpopulation robustness with COAR-EDIT.** We edit pre-trained ResNet-50 models to improve their worst-subpopulation accuracy on two benchmark datasets: Waterbirds [SKH+20] and CelebA [LLW+15]. Before applying COAR-EDIT, models fine-tuned on Waterbirds and CelebA attain 87% and 96% test accuracy but only 64% and 47% accuracy on their worst-performing subpopulations, respectively. On the left, applying COAR-EDIT by ablating 210 of 22,720 components in the Waterbirds model increases worst-subpopulation accuracy from 64% to 83% without degrading its accuracy averaged over examples (light blue) and subpopulations (dark blue). Similarly, on the right, editing the CelebA model by ablating a targeted subset of 26 components improves worst-subpopulation accuracy from 47% to 85%.

5.3 Improving subpopulation robustness

Machine learning models often latch onto spurious correlations in the training dataset [GRM+19; STR+20; HMF+23], resulting in subpar performance on subpopulations where these correlations do not hold [BG18; ODC+20]. In this section, we test whether our editing approach can boost performance on such underperforming subpopulations without degrading overall performance.

In particular, we evaluate COAR-EDIT on two benchmark datasets—Waterbirds [SKH+20] and CelebA [LLW+15]—where models fare poorly on subpopulations that are underrepresented in the training data. On both datasets, our goal is to improve a given model’s *worst-subpopulation accuracy*—we defer experiment details to Appendix D.3.

Results. On both datasets, COAR successfully identifies component subsets that correspond to effective model edits. Figure 5 depicts our results. On Waterbirds (Figure 5a), ablating 210 components (0.9% of all components) improves worst-subpopulation accuracy from 64% to 83% (red) without degrading its accuracy averaged uniformly over examples (light blue) and subpopulations (dark blue). On CelebA, Figure 5b demonstrates that zeroing out 26 of 22,720 model components improves worst-subpopulation accuracy from 47% to 85% and average-subpopulation accuracy from 84% to 90% while only incurring a 5% drop in test set accuracy.

Before continuing, we make two observations. First, on both datasets, our editing-based approach is *sample-efficient*—it does not require subpopulation-level annotations for the training set, and only uses 20 random training examples from each subpopulation to find effective model edits. Second, our results indicate that simply ablating a few components from models trained via “standard” empirical risk minimization (ERM) can achieve worst-subpopulation accuracy improvements that are comparable to gains from specialized methods (e.g., based on robust optimization [SKH+20], dataset balancing [IAP+22], and generative modeling [GGL+20]).

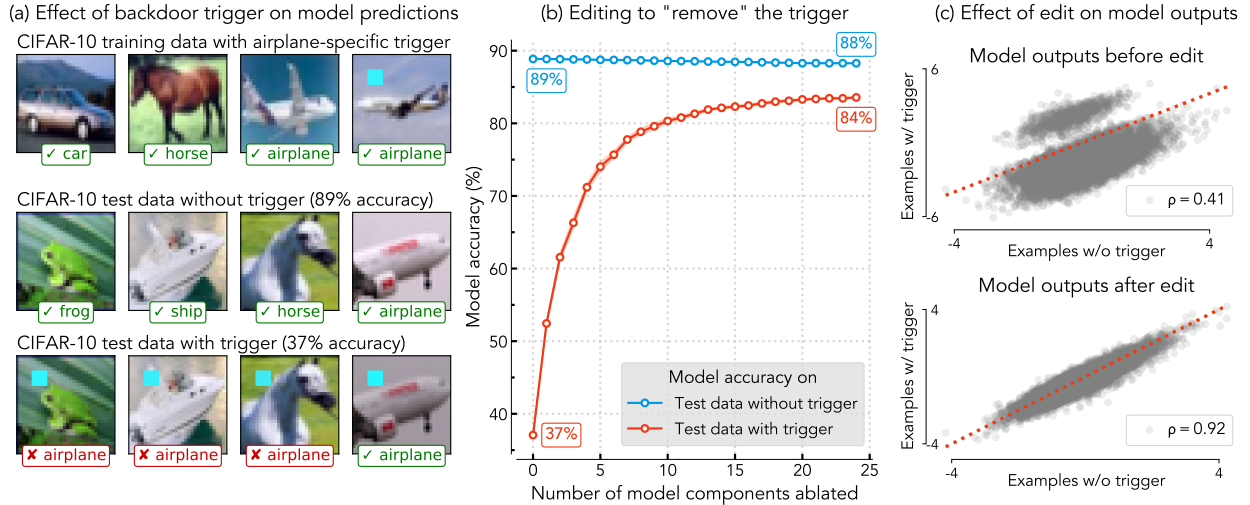


Figure 6: **Localizing backdoor attacks with COAR-EDIT.** We edit a ResNet18 model trained on a backdoored CIFAR-10 dataset in which half of all training examples in the “airplane” class contain a planted blue-squared trigger. On the left, we find that the model is sensitive to the trigger—backdoor attacks that add the trigger to examples drop test accuracy from 89% (middle row) to 37% (bottom row). In the center panel, we apply COAR-EDIT to identify 25 backdoor-specific components that, when ablated, boost accuracy on examples with the trigger (red) from 37% to 84% without impacting accuracy on examples without the trigger (blue). On the right, we find that the edit suppresses sensitivity to the trigger even at the example level—the correlation between model outputs on paired examples with and without the trigger increases from 0.41 to 0.92.

5.4 Localizing backdoor attacks

We now use COAR-EDIT to analyze the sensitivity of model predictions to backdoor attacks [BNL12; GDG17], where an adversary plants a spurious correlation in the training dataset and uses it as a trigger to override predictions at test time. In this experiment, we first train a ResNet18 model on a modified CIFAR-10 dataset in which half of the training examples in the “airplane” class contain a planted blue-squared trigger, as shown in Figure 6a. Then, using COAR-EDIT, we evaluate whether the effect of this trigger on predictions can be localized to a few components, which, if ablated, induces model robustness to backdoor attacks without degrading overall performance.

Results. Figure 6 summarizes our findings. Figure 6a shows that prior to editing, the model trained on the modified CIFAR-10 dataset (top row) is sensitive to backdoor attacks—simply adding the “airplane” trigger to test examples drops model accuracy from 89% (middle row) to 37% (bottom row). To localize the effect of the trigger, we use COAR-EDIT over ten *paired* examples—i.e., examples with and without the backdoor trigger—to identify a few components that, when ablated, correct the misclassifications induced by the trigger without impacting predictions on test examples without the trigger. In Figure 6b, we find that editing the model by ablating 25 components (1%) is sufficient to boost accuracy on test examples with the trigger (red) from 37% to 84% without impacting accuracy on examples without the trigger (blue) by more than 1%. Figure 6c shows that the edit suppresses the effect of the trigger at the example level as well, improving correlation between model outputs on examples with and without the trigger from 0.41 (top row) to 0.92 (bottom row). We defer additional details and analyses to Appendix D.4.

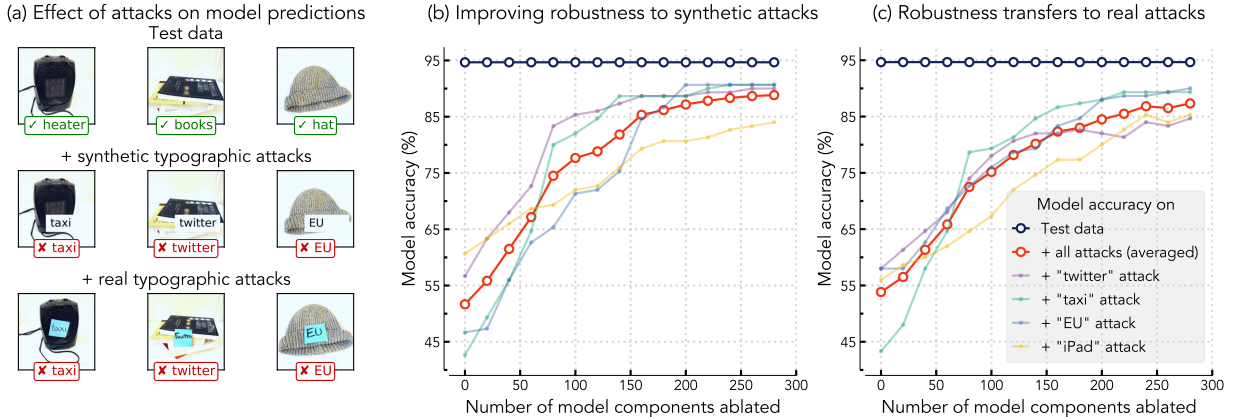


Figure 7: **Improving robustness to typographic attacks with COAR-EDIT.** We edit a zero-shot CLIP ViT-B/16 classifier to improve its robustness to typographic attacks [GCV+21]. On the left, we find that predictions on images of household objects (top row) can be manipulated to “taxi”, “twitter”, or “EU” via synthetic (middle row) and real (last row) typographic attacks. In the center panel, we use COAR-EDIT to identify components that, when ablated, improve average accuracy on examples with synthetic typographic attacks (red) from 51% to 89% while maintaining accuracy on examples without attacks (blue). Similarly, on the right, we find that the edit transfers robustness to real typographic attacks as well, improving average accuracy from 54% to 86%.

5.5 Improving robustness to typographic attacks

Zero-shot CLIP classifiers are vulnerable to typographic attacks [GCV+21] that simply insert text to images in order to induce misclassifications. In this experiment, we evaluate whether our editing approach can improve the robustness of a zero-shot CLIP ViT-B/16 classifier using a dataset [MTB22] comprising 180 images with and without multiple typographic attacks. Specifically, we use COAR-EDIT to identify a subset of components that, when ablated, correct the misclassifications induced by synthetic typographic attacks without impacting predictions on images without attacks. We defer additional details to Appendix D.5.

Results. Figure 7 summarizes our findings. In Figure 7a, we show that the predictions of a zero-shot CLIP ViT-B/16 classifier on images of household objects (top row) can be manipulated to “taxi”, “twitter”, or “EU” via synthetic (middle row) or real (last row) typographic attacks. More quantitatively, we find that the zero-shot accuracy on images with synthetic and real typographic attacks drops from 95% to 51% and 54%, respectively. Figure 7b shows that ablating a subset of 300 components (0.4%) identified via COAR-EDIT improves the accuracy on held-out images with synthetic typographic attacks from 51% to 89% on average (red), without impacting accuracy on images without attacks (dark blue). Furthermore, in Figure 7c, we find that our edit transfers robustness to real typographic attacks as well, improving accuracy on held-out images from 54% to 86% on average. Similar to previous experiments, our approach is sample-efficient in that it only requires 15 pairs of target and reference examples with and without synthetic attacks to identify the edit described above.

To summarize, simply ablating targeted subsets of components identified via COAR-EDIT can induce specific model behavior without requiring additional training. More broadly, our findings highlight how accurate component attribution *alone* can directly inform model editing.

6 Related work

Our work relates to multiple topics in interpretability, which we categorize into works that focus on localizing model behavior, interpreting individual components, editing models, and approximating functional behavior via interpretable proxies.

Localizing model behavior. One line of work in mechanistic interpretability attempts to identify “circuits” [OCS+20b] or “subnetworks” [CSR21] within neural networks that are responsible for specific capabilities or biases such as factual recall [MBA+22], gender bias [VGB+20], or arithmetic reasoning [SBS23]. Building on this, several works focus on automated localization of behavior using techniques such as fine-tuning [PSZ+23], activation patching [CML+23; GMS+23], or differentiable masking [BFC+23; DSH+21; CTJ23]. More recent studies evaluate these methods in terms of their sensitivity to design choices [ZN23], usefulness for model editing [HBK+23], and ability to characterize functional behavior [WLL+23]. Other works develop metrics to quantify the “importance” of individual components (e.g., [DSY18; LSD+18; GZ20]), which we adapt as baselines in Section 4. Rather than localizing human-defined behavior to specific components, the component modeling task (Definition 2) aims to explicitly model the collective function mapping component ablations to predictions.

Interpreting specific model components. The works discussed above aim to localize specific model behavior to components; another line of work studies the reverse direction, and introduces methods for uncovering the functionality corresponding to a specific model component. Such methods include feature visualization [ZF14; GKB+22], activation maps [BZK+17; MA20], ablations [ZSB+18], saliency maps [OSJ+18], probing [DDS+19; DSD+20], and natural language descriptions [HSB+21; OW22; BCM+23]. Subsequent analyses use these methods to identify and ascribe meaning to specific model components by labeling them as, e.g., “curve detectors” [CGC+20], “knowledge neurons” [DDH+21], “multimodal neurons” [GCV+21], or “syntax units” [LKD+19]. More recent work revisits the reliability and robustness of such methods [GZB+23; BPY+21; HEK+18; SJN21; HL19; AB21; HGD+23]. Here, our goal is not to interpret specific model components, but rather to study how all components jointly influence model predictions through the lens of component modeling (Definition 1).

Editing model behavior. Another related line of work focuses on *model editing*, the goal of which is to make small, targeted changes to model representations in order to induce or suppress a specific behavior. Model editing methods include “hypernetworks” [DAT21; MLB+21], rank-one updates to model parameters [BLW+20; STE+21; MBA+22], constrained fine-tuning [ZRZ+20], and weight interpolation [IRW+22; ZPC+23], among other methods. Recent work has also studied erasing concepts and suppressing spurious correlations from models using layer-wise linear probing [RTG+22], CLIP-specific methods [GES23; CYV+23], and fine-tuning variants [GMF+23; KIW22]. In this work, we introduce COAR-EDIT to show that effective component attribution can directly enable model editing at the level of examples (§5.1), classes (§5.2), subpopulations (§5.3), and spurious concepts (§5.4, §5.5) by zeroing out targeted subsets of components.

Understanding machine learning models by proxy. More generally, our approach connects to a line of research that aims to understand machine learning models by constructing *interpretable proxies*. For example, feature attribution methods like LIME [RSG16] approximate a given ML model with a linear model in input space. Similarly, datamodeling [IPE+22] approximates a given learning algorithm by a linear model in “dataset space.” Another line of work analyzes the behavior of deep networks via high-level causal abstractions [GLI+21; GPI23], user-specified causal graphs over task-specific variables.

7 Discussion

In this section, we discuss connections between component attribution and model editing, discuss directions for future work, and outline key limitations of COAR.

Does localization help with model editing? The extent to which localizing specific model behavior to a subset of model components helps with model editing remains contested. On one hand, Hase et al. [HBK+23] show that localizing factual associations in language models does not necessarily help with editing these associations. More broadly, recent evaluation studies suggest that model editing can degrade robustness to distribution shifts [BGN+23] and may not modify model behavior in a consistent manner [CBY+23]. On the other hand, recent work shows that some localization methods can in fact recover ground-truth localization in controlled settings [CTJ23] and improve calibration of fine-tuned language models [PSZ+23]. Our findings in Section 5 substantiate the latter view, as COAR-EDIT uses component attributions to identify a target subset of components that, when ablated, modify model behavior as intended.

Future work. We highlight three directions that, while outside the scope of this work, may be interesting avenues for future work.

- **Analyzing neural network representations.** An interesting direction for future work could be to use component attribution (and component models, more generally) to study empirically documented phenomena in deep learning. There are a plethora of questions to ask here which, although beyond the scope of this work, are natural applications of component attributions. For example, extending our results from Section 5.1, can we use component attribution to better isolate “opposing signals” [RR23] for a given task, and to understand their role in shaping model predictions? Can we use component attributions to study how model predictions change due to adversarial perturbations [GSS15], or over the course of training [KKN+19]? Similarly, can we develop improved methods for localizing memorized inputs to specific model components [FZ20; MMS+23]? Given that component attributions are causally meaningful, can we use them as a kernel with which to compare different models [KNL+19] or learning algorithms [SPI+23]?
- **Attributing generative models.** While we focus on vision models in this work, COAR is a general method that can estimate component attributions for any machine learning model. Future work might thus explore possible model output functions (and their corresponding component attributions) for *generative* models. For diffusion-based generative models, one might study the denoising error for a fixed timestep, as in [GVS+23; ZPD+23]. For language models, a possible point of start (following Park et al. [PGI+23]) would be to use the average correct-class margin (5) of a sequence of tokens as the model output function. Our preliminary experiments in Appendix B show that COAR learns accurate component attributions for language models such as GPT-2 [RWC+19] and Phi-2 [LBE+23]. In general, estimating and applying component attributions for generative models is a promising avenue for future work.
- **Beyond linear component attribution.** The fact that component attributions’ predictiveness decreases on out-of-distribution component subsets, i.e., when $\alpha_{\text{test}} \neq \alpha_{\text{train}}$, suggests that the linear form of component attributions might not be expressive enough to fully capture the map between model components and outputs. Given the generality of COAR, an interesting avenue for future work would be to explore whether non-linear component models such as decision trees or kernel methods predict component counterfactuals more accurately, and as a result, improve model editing.

Limitations. Our attribution-based approach for decomposing and editing model predictions is not without its limitations. First, estimating COAR attributions involves constructing datasets of ground-truth counterfactuals (Equation 2), which can require a large number of forward passes through the model. In Appendix C.5, we show that simply using 2-5 \times fewer samples can significantly speed up COAR without impacting the quality of the resulting attributions. Mitigating this computational bottleneck further through better sampling or approximation techniques is an interesting avenue for future work. Second, COAR requires specifying an ablation method (Equation 1). While we use zero ablations in this work (Remark 2), one could also use COAR with ablation methods (e.g., Chan et al. [CGG+22]) that account for distribution shifts in activation space. For example, in Appendix C.4, we show that COAR yields predictive attributions with another ablation method that simply scales down the activations of ablated components by a small constant factor instead of setting them to zero. Finally, as noted in Remark 4, our model editing approach COAR is coarse-grained in that it modifies model behavior by simply ablating a targeted subset of components. Using COAR in conjunction with gradient-based editing techniques in order to make finer-grained model edits is an interesting avenue for future work.

8 Conclusion

We first formalize the problem of decomposing model predictions in terms of model components through the *component modeling* task. We specifically focus on a special case of component modeling, *component attribution*, where the goal is to predict the counterfactual impact of every component on a given prediction. We then propose COAR, a scalable method for estimating predictive component attributions, and demonstrate its effectiveness across model architectures, datasets, and tasks. Finally, through a series of five experiments, we also stress-test the utility of COAR attributions in directly editing model behavior without requiring additional training.

Acknowledgements

The authors would like to thank Benjamin Cohen-Wang, Logan Engstrom, Alaa Khaddaj, and Kristian Georgiev for helpful discussions and comments on an earlier draft of this manuscript.

Work supported in part by the NSF grant DMS-2134108. This material is based upon work supported by the Defense Advanced Research Projects Agency (DARPA) under Contract No. HR001120C0015.

References

- [AB16] Guillaume Alain and Yoshua Bengio. “Understanding intermediate layers using linear classifier probes”. In: *arXiv preprint arXiv:1610.01644* (2016).
- [AB21] Omer Antverg and Yonatan Belinkov. “On the pitfalls of analyzing individual neurons in language models”. In: *arXiv preprint arXiv:2110.07483* (2021).
- [Bau74] Friedrich L Bauer. “Computational graphs and rounding error”. In: *SIAM Journal on Numerical Analysis*. Vol. 11. 1. SIAM, 1974, pp. 87–96.
- [BCM+23] Steven Bills, Nick Cammarata, Dan Mossing, Henk Tillman, Leo Gao, Gabriel Goh, Ilya Sutskever, Jan Leike, Jeff Wu, and William Saunders. “Language models can explain neurons in language models”. In: URL <https://openaipublic.blob.core.windows.net/neuron-explainer/paper/index.html>. (Date accessed: 14.05. 2023) (2023).
- [BFC+23] Deniz Bayazit, Negar Foroutan, Zeming Chen, Gail Weiss, and Antoine Bosselut. “Discovering Knowledge-Critical Subnetworks in Pretrained Language Models”. In: *arXiv preprint arXiv:2310.03084* (2023).
- [BG18] Joy Buolamwini and Timnit Gebru. “Gender shades: Intersectional accuracy disparities in commercial gender classification”. In: *Conference on fairness, accountability and transparency (FAcT)*. 2018.
- [BGN+23] Davis Brown, Charles Godfrey, Cody A. Nizinski, Jonathan Tu, and Henry Kvinge. “Robustness of edited neural networks”. In: *ArXiv abs/2303.00046* (2023).
- [BLW+20] David Bau, Steven Liu, Tongzhou Wang, Jun-Yan Zhu, and Antonio Torralba. “Rewriting a deep generative model”. In: *European Conference on Computer Vision (ECCV)*. 2020.
- [BLZ18] Terra Blevins, Omer Levy, and Luke Zettlemoyer. “Deep RNNs encode soft hierarchical syntax”. In: *arXiv preprint arXiv:1805.04218* (2018).
- [BNL12] Battista Biggio, Blaine Nelson, and Pavel Laskov. “Poisoning attacks against support vector machines”. In: *International Conference on Machine Learning*. 2012.
- [BPY+21] Tolga Bolukbasi, Adam Pearce, Ann Yuan, Andy Coenen, Emily Reif, Fernanda Viégas, and Martin Wattenberg. “An interpretability illusion for bert”. In: *arXiv preprint arXiv:2104.07143* (2021).
- [BVP18] Sara Beery, Grant Van Horn, and Pietro Perona. “Recognition in terra incognita”. In: *European Conference on Computer Vision (ECCV)*. 2018.
- [BZK+17] David Bau, Bolei Zhou, Aditya Khosla, Aude Oliva, and Antonio Torralba. “Network dissection: Quantifying interpretability of deep visual representations”. In: *Computer Vision and Pattern Recognition (CVPR)*. 2017.
- [BZS+20] David Bau, Jun-Yan Zhu, Hendrik Strobelt, Agata Lapedriza, Bolei Zhou, and Antonio Torralba. “Understanding the role of individual units in a deep neural network”. In: *Proceedings of the National Academy of Sciences (PNAS)* (2020).
- [CBY+23] Roi Cohen, Eden Biran, Ori Yoran, Amir Globerson, and Mor Geva. “Evaluating the Ripple Effects of Knowledge Editing in Language Models”. In: *ArXiv abs/2307.12976* (2023).
- [CGC+20] Nick Cammarata, Gabriel Goh, Shan Carter, Ludwig Schubert, Michael Petrov, and Chris Olah. “Curve detectors”. In: *Distill* 5.6 (2020), e00024–003.

- [CGG+22] Lawrence Chan, Adrià Garriga-Alonso, Nicholas Goldowsky-Dill, Ryan Greenblatt, Jenny Nitishinskaya, Ansh Radhakrishnan, Buck Shlegeris, and Nate Thomas. “Causal scrubbing: A method for rigorously testing interpretability hypotheses”. In: 2022.
- [CLC+19] Christopher Clark, Kenton Lee, Ming-Wei Chang, Tom Kwiatkowski, Michael Collins, and Kristina Toutanova. “BoolQ: Exploring the surprising difficulty of natural yes/no questions”. In: *arXiv preprint arXiv:1905.10044* (2019).
- [CML+23] Arthur Conmy, Augustine N Mavor-Parker, Aengus Lynch, Stefan Heimersheim, and Adrià Garriga-Alonso. “Towards automated circuit discovery for mechanistic interpretability”. In: *arXiv preprint arXiv:2304.14997* (2023).
- [CSR21] Steven Cao, Victor Sanh, and Alexander M Rush. “Low-complexity probing via finding subnetworks”. In: *arXiv preprint arXiv:2104.03514* (2021).
- [CTJ23] Ting-Yun Chang, Jesse Thomason, and Robin Jia. “Do Localization Methods Actually Localize Memorized Data in LLMs?” In: *arXiv preprint arXiv:2311.09060* (2023).
- [CYV+23] Haozhe Chen, Junfeng Yang, Carl Vondrick, and Chengzhi Mao. “Interpreting and Controlling Vision Foundation Models via Text Explanations”. In: *arXiv preprint arXiv:2310.10591* (2023).
- [DAT21] Nicola De Cao, Wilker Aziz, and Ivan Titov. “Editing factual knowledge in language models”. In: *arXiv preprint arXiv:2104.08164* (2021).
- [DBK+21] Alexey Dosovitskiy, Lucas Beyer, Alexander Kolesnikov, Dirk Weissenborn, Xiaohua Zhai, Thomas Unterthiner, Mostafa Dehghani, Matthias Minderer, Georg Heigold, Sylvain Gelly, et al. “An image is worth 16x16 words: Transformers for image recognition at scale”. In: *International Conference on Learning Representations (ICLR)*. 2021.
- [DDH+21] Damai Dai, Li Dong, Yaru Hao, Zhifang Sui, Baobao Chang, and Furu Wei. “Knowledge neurons in pretrained transformers”. In: *arXiv preprint arXiv:2104.08696* (2021).
- [DDS+09] Jia Deng, Wei Dong, Richard Socher, Li-Jia Li, Kai Li, and Li Fei-Fei. “Imagenet: A large-scale hierarchical image database”. In: *Computer Vision and Pattern Recognition (CVPR)*. 2009.
- [DDS+19] Fahim Dalvi, Nadir Durrani, Hassan Sajjad, Yonatan Belinkov, Anthony Bau, and James Glass. “What is one grain of sand in the desert? analyzing individual neurons in deep nlp models”. In: *Proceedings of the AAAI Conference on Artificial Intelligence*. Vol. 33. 01. 2019, pp. 6309–6317.
- [DSD+20] Nadir Durrani, Hassan Sajjad, Fahim Dalvi, and Yonatan Belinkov. “Analyzing individual neurons in pre-trained language models”. In: *arXiv preprint arXiv:2010.02695* (2020).
- [DSH+21] Nicola De Cao, Leon Schmid, Dieuwke Hupkes, and Ivan Titov. “Sparse interventions in language models with differentiable masking”. In: *arXiv preprint arXiv:2112.06837* (2021).
- [DSY18] Kedar Dhamdhere, Mukund Sundararajan, and Qiqi Yan. “How important is a neuron?” In: *arXiv preprint arXiv:1805.12233* (2018).
- [EHO+22] Nelson Elhage, Tristan Hume, Catherine Olsson, Nicholas Schiefer, Tom Henighan, Shauna Kravec, Zac Hatfield-Dodds, Robert Lasenby, Dawn Drain, Carol Chen, et al. “Toy models of superposition”. In: *arXiv preprint arXiv:2209.10652* (2022).

- [EL23] Ronen Eldan and Yuanzhi Li. “TinyStories: How Small Can Language Models Be and Still Speak Coherent English?” In: *arXiv preprint arXiv:2305.07759* (2023).
- [FZ20] Vitaly Feldman and Chiyuan Zhang. “What Neural Networks Memorize and Why: Discovering the Long Tail via Influence Estimation”. In: *Advances in Neural Information Processing Systems (NeurIPS)*. Vol. 33. 2020, pp. 2881–2891.
- [GCV+21] Gabriel Goh, Nick Cammarata, Chelsea Voss, Shan Carter, Michael Petrov, Ludwig Schubert, Alec Radford, and Chris Olah. “Multimodal neurons in artificial neural networks”. In: *Distill* (2021).
- [GDG17] Tianyu Gu, Brendan Dolan-Gavitt, and Siddharth Garg. “Badnets: Identifying Vulnerabilities in the Machine Learning Model Supply Chain”. In: *arXiv preprint arXiv:1708.06733* (2017).
- [GES23] Yossi Gandelsman, Alexei A Efros, and Jacob Steinhardt. “Interpreting CLIP’s Image Representation via Text-Based Decomposition”. In: *arXiv preprint arXiv:2310.05916* (2023).
- [GGL+20] Karan Goel, Albert Gu, Yixuan Li, and Christopher Ré. “Model patching: Closing the subgroup performance gap with data augmentation”. In: *arXiv preprint arXiv:2008.06775* (2020).
- [GJM+20] Robert Geirhos, Jörn-Henrik Jacobsen, Claudio Michaelis, Richard Zemel, Wieland Brendel, Matthias Bethge, and Felix A Wichmann. “Shortcut learning in deep neural networks”. In: *Nature Machine Intelligence*. 2020.
- [GKB+22] Amin Ghiasi, Hamid Kazemi, Eitan Borgnia, Steven Reich, Manli Shu, Micah Goldblum, Andrew Gordon Wilson, and Tom Goldstein. “What do vision transformers learn? a visual exploration”. In: *arXiv preprint arXiv:2212.06727* (2022).
- [GLI+21] Atticus Geiger, Hanson Lu, Thomas Icard, and Christopher Potts. “Causal abstractions of neural networks”. In: *Advances in Neural Information Processing Systems* 34 (2021), pp. 9574–9586.
- [GMF+23] Rohit Gandikota, Joanna Materzynska, Jaden Fiotto-Kaufman, and David Bau. “Erasing concepts from diffusion models”. In: *arXiv preprint arXiv:2303.07345* (2023).
- [GMS+23] Nicholas Goldowsky-Dill, Chris MacLeod, Lucas Sato, and Aryaman Arora. “Localizing model behavior with path patching”. In: *arXiv preprint arXiv:2304.05969* (2023).
- [GPI23] Atticus Geiger, Chris Potts, and Thomas Icard. “Causal abstraction for faithful model interpretation”. In: *arXiv preprint arXiv:2301.04709* (2023).
- [GRM+19] Robert Geirhos, Patricia Rubisch, Claudio Michaelis, Matthias Bethge, Felix A. Wichmann, and Wieland Brendel. “ImageNet-trained CNNs are biased towards texture; increasing shape bias improves accuracy and robustness.” In: *International Conference on Learning Representations (ICLR)*. 2019.
- [GSS15] Ian J Goodfellow, Jonathon Shlens, and Christian Szegedy. “Explaining and Harnessing Adversarial Examples”. In: *International Conference on Learning Representations (ICLR)*. 2015.

- [GTA+23] Leo Gao, Jonathan Tow, Baber Abbasi, Stella Biderman, Sid Black, Anthony DiPofi, Charles Foster, Laurence Golding, Jeffrey Hsu, Alain Le Noac’h, Haonan Li, Kyle McDonell, Niklas Muennighoff, Chris Ociepa, Jason Phang, Laria Reynolds, Hailey Schoelkopf, Aviya Skowron, Lintang Sutawika, Eric Tang, Anish Thite, Ben Wang, Kevin Wang, and Andy Zou. *A framework for few-shot language model evaluation*. Version v0.4.0. Dec. 2023. DOI: [10.5281/zenodo.10256836](https://doi.org/10.5281/zenodo.10256836). URL: <https://zenodo.org/records/10256836>.
- [GVS+23] Kristian Georgiev, Joshua Vendrow, Hadi Salman, Sung Min Park, and Aleksander Madry. “The journey, not the destination: How data guides diffusion models”. In: *arXiv preprint arXiv:2312.06205* (2023).
- [GZ20] Amirata Ghorbani and James Y Zou. “Neuron shapley: Discovering the responsible neurons”. In: *Advances in neural information processing systems* 33 (2020), pp. 5922–5932.
- [GZB+23] Robert Geirhos, Roland S Zimmermann, Blair Bilodeau, Wieland Brendel, and Been Kim. “Don’t trust your eyes: on the (un) reliability of feature visualizations”. In: *arXiv preprint arXiv:2306.04719* (2023).
- [HBK+23] Peter Hase, Mohit Bansal, Been Kim, and Asma Ghandeharioun. “Does localization inform editing? surprising differences in causality-based localization vs. knowledge editing in language models”. In: *arXiv preprint arXiv:2301.04213* (2023).
- [HD19] Dan Hendrycks and Thomas G. Dietterich. “Benchmarking Neural Network Robustness to Common Corruptions and Surface Variations”. In: *International Conference on Learning Representations (ICLR)*. 2019.
- [HEK+18] Sara Hooker, Dumitru Erhan, Pieter-Jan Kindermans, and Been Kim. “A benchmark for interpretability methods in deep neural networks”. In: *arXiv preprint arXiv:1806.10758* (2018).
- [HGD+23] Jing Huang, Atticus Geiger, Karel D’Oosterlinck, Zhengxuan Wu, and Christopher Potts. “Rigorously Assessing Natural Language Explanations of Neurons”. In: *arXiv preprint arXiv:2309.10312* (2023).
- [HL19] John Hewitt and Percy Liang. “Designing and interpreting probes with control tasks”. In: *arXiv preprint arXiv:1909.03368* (2019).
- [HMF+23] Katherine L Hermann, Hossein Mobahi, Thomas Fel, and Michael C Mozer. “On the Foundations of Shortcut Learning”. In: *arXiv preprint arXiv:2310.16228* (2023).
- [HSB+21] Evan Hernandez, Sarah Schwettmann, David Bau, Teona Bagashvili, Antonio Torralba, and Jacob Andreas. “Natural language descriptions of deep visual features”. In: *International Conference on Learning Representations*. 2021.
- [HSP+22] Thomas Hartvigsen, Swami Sankaranarayanan, Hamid Palangi, Yoon Kim, and Marzyeh Ghassemi. “Aging with GRACE: Lifelong Model Editing with Discrete Key-Value Adaptors”. In: *arXiv preprint arXiv:2211.11031* (2022).
- [HSZ+23] Zeyu Huang, Yikang Shen, Xiaofeng Zhang, Jie Zhou, Wenge Rong, and Zhang Xiong. “Transformer-Patcher: One Mistake worth One Neuron”. In: *arXiv preprint arXiv:2301.09785* (2023).
- [HZR+15] Kaiming He, Xiangyu Zhang, Shaoqing Ren, and Jian Sun. *Deep Residual Learning for Image Recognition*. 2015.

- [IAP+22] Badr Youbi Idrissi, Martin Arjovsky, Mohammad Pezeshki, and David Lopez-Paz. “Simple data balancing achieves competitive worst-group-accuracy”. In: *Conference on Causal Learning and Reasoning*. PMLR. 2022, pp. 336–351.
- [IPE+22] Andrew Ilyas, Sung Min Park, Logan Engstrom, Guillaume Leclerc, and Aleksander Madry. “Datamodels: Predicting Predictions from Training Data”. In: *International Conference on Machine Learning (ICML)*. 2022.
- [IRW+22] Gabriel Ilharco, Marco Tulio Ribeiro, Mitchell Wortsman, Suchin Gururangan, Ludwig Schmidt, Hannaneh Hajishirzi, and Ali Farhadi. “Editing models with task arithmetic”. In: *arXiv preprint arXiv:2212.04089* (2022).
- [JB23] Mojan Javaheripi and Sébastien Bubeck. *Phi-2: The surprising power of small language models*. Dec. 2023. URL: <https://www.microsoft.com/en-us/research/blog/phi-2-the-surprising-power-of-small-language-models/>.
- [JPG+19] Alistair EW Johnson, Tom J Pollard, Nathaniel R Greenbaum, Matthew P Lungren, Chih-ying Deng, Yifan Peng, Zhiyong Lu, Roger G Mark, Seth J Berkowitz, and Steven Horng. “MIMIC-CXR-JPG, a large publicly available database of labeled chest radiographs”. In: *arXiv preprint arXiv:1901.07042* (2019).
- [KIW22] Polina Kirichenko, Pavel Izmailov, and Andrew Gordon Wilson. “Last layer re-training is sufficient for robustness to spurious correlations”. In: *arXiv preprint arXiv:2204.02937* (2022).
- [KKN+19] Dimitris Kalimeris, Gal Kaplun, Preetum Nakkiran, Benjamin Edelman, Tristan Yang, Boaz Barak, and Haofeng Zhang. “Sgd on neural networks learns functions of increasing complexity”. In: *Advances in neural information processing systems* 32 (2019).
- [KLS+24] János Kramár, Tom Lieberum, Rohin Shah, and Neel Nanda. “AtP*: An efficient and scalable method for localizing LLM behaviour to components”. In: *arXiv preprint arXiv:2403.00745* (2024).
- [KMM+20] Narine Kokhlikyan, Vivek Miglani, Miguel Martin, Edward Wang, Bilal Alsallakh, Jonathan Reynolds, Alexander Melnikov, Natalia Kliushkina, Carlos Araya, Siqi Yan, et al. “Captum: A unified and generic model interpretability library for pytorch”. In: *arXiv preprint arXiv:2009.07896* (2020).
- [KNL+19] Simon Kornblith, Mohammad Norouzi, Honglak Lee, and Geoffrey Hinton. “Similarity of Neural Network Representations Revisited”. In: *Proceedings of the 36th International Conference on Machine Learning (ICML)*. 2019.
- [Kri09] Alex Krizhevsky. “Learning Multiple Layers of Features from Tiny Images”. In: *Technical report*. 2009.
- [LBE+23] Yuanzhi Li, Sébastien Bubeck, Ronen Eldan, Allie Del Giorno, Suriya Gunasekar, and Yin Tat Lee. “Textbooks are all you need ii: phi-1.5 technical report”. In: *arXiv preprint arXiv:2309.05463* (2023).
- [LIE+22] Guillaume Leclerc, Andrew Ilyas, Logan Engstrom, Sung Min Park, Hadi Salman, and Aleksander Madry. *ffcv*. <https://github.com/libffcv/ffcv/>. 2022.
- [LKD+19] Yair Lakretz, German Kruszewski, Theo Desbordes, Dieuwke Hupkes, Stanislas Dehaene, and Marco Baroni. “The emergence of number and syntax units in LSTM language models”. In: *arXiv preprint arXiv:1903.07435* (2019).
- [LLW+15] Ziwei Liu, Ping Luo, Xiaogang Wang, and Xiaoou Tang. “Deep Learning Face Attributes in the Wild”. In: *International Conference on Computer Vision (ICCV)*. 2015.

- [LSD+18] Klas Leino, Shayak Sen, Anupam Datta, Matt Fredrikson, and Linyi Li. “Influence-directed explanations for deep convolutional networks”. In: *2018 IEEE international test conference (ITC)*. IEEE. 2018, pp. 1–8.
- [LYS+20] Yuezun Li, Xin Yang, Pu Sun, Honggang Qi, and Siwei Lyu. “Celeb-df: A large-scale challenging dataset for deepfake forensics”. In: *Proceedings of the IEEE/CVF conference on computer vision and pattern recognition*. 2020, pp. 3207–3216.
- [MA20] Jesse Mu and Jacob Andreas. “Compositional explanations of neurons”. In: *Advances in Neural Information Processing Systems* 33 (2020), pp. 17153–17163.
- [MBA+22] Kevin Meng, David Bau, Alex Andonian, and Yonatan Belinkov. “Locating and Editing Factual Associations in GPT”. In: *Advances in Neural Information Processing Systems* 36 (2022).
- [MLB+21] Eric Mitchell, Charles Lin, Antoine Bosselut, Chelsea Finn, and Christopher D Manning. “Fast model editing at scale”. In: *arXiv preprint arXiv:2110.11309* (2021).
- [MMS+23] Pratyush Maini, Michael C Mozer, Hanie Sedghi, Zachary C Lipton, J Zico Kolter, and Chiyuan Zhang. “Can Neural Network Memorization Be Localized?” In: *International Conference on Machine Learning*. 2023.
- [MTB22] Joanna Materzyńska, Antonio Torralba, and David Bau. “Disentangling visual and written concepts in clip”. In: *Proceedings of the IEEE/CVF Conference on Computer Vision and Pattern Recognition*. 2022, pp. 16410–16419.
- [NCL+23] Neel Nanda, Lawrence Chan, Tom Liberum, Jess Smith, and Jacob Steinhardt. “Progress measures for grokking via mechanistic interpretability”. In: *arXiv preprint arXiv:2301.05217* (2023).
- [OCS+20a] Chris Olah, Nick Cammarata, Ludwig Schubert, Gabriel Goh, Michael Petrov, and Shan Carter. “An Overview of Early Vision in InceptionV1”. In: *Distill* (2020). DOI: [10.23915/distill.00024.002](https://doi.org/10.23915/distill.00024.002).
- [OCS+20b] Chris Olah, Nick Cammarata, Ludwig Schubert, Gabriel Goh, Michael Petrov, and Shan Carter. “Zoom In: An Introduction to Circuits”. In: *Distill* (2020). DOI: [10.23915/distill.00024.001](https://doi.org/10.23915/distill.00024.001).
- [ODC+20] Lauren Oakden-Rayner, Jared Dunnmon, Gustavo Carneiro, and Christopher Ré. “Hidden stratification causes clinically meaningful failures in machine learning for medical imaging”. In: *Proceedings of the ACM conference on health, inference, and learning*. 2020.
- [OEN+22] Catherine Olsson, Nelson Elhage, Neel Nanda, Nicholas Joseph, Nova DasSarma, Tom Henighan, Ben Mann, Amanda Askell, Yuntao Bai, Anna Chen, et al. “In-context learning and induction heads”. In: *arXiv preprint arXiv:2209.11895* (2022).
- [OSJ+18] Chris Olah, Arvind Satyanarayan, Ian Johnson, Shan Carter, Ludwig Schubert, Katherine Ye, and Alexander Mordvintsev. “The Building Blocks of Interpretability”. In: *Distill*. 2018.
- [OW22] Tuomas Oikarinen and Tsui-Wei Weng. “Clip-dissect: Automatic description of neuron representations in deep vision networks”. In: *arXiv preprint arXiv:2204.10965* (2022).
- [PGI+23] Sung Min Park, Kristian Georgiev, Andrew Ilyas, Guillaume Leclerc, and Aleksander Madry. “TRAK: Attributing Model Behavior at Scale”. In: *Arxiv preprint arXiv:2303.14186*. 2023.

- [PSZ+23] Abhishek Panigrahi, Nikunj Saunshi, Haoyu Zhao, and Sanjeev Arora. "Task-Specific Skill Localization in Fine-tuned Language Models". In: *arXiv preprint arXiv:2302.06600* (2023).
- [RJS17] Alec Radford, Rafal Jozefowicz, and Ilya Sutskever. "Learning to generate reviews and discovering sentiment". In: *arXiv preprint arXiv:1704.01444* (2017).
- [RKH+21] Alec Radford, Jong Wook Kim, Chris Hallacy, Aditya Ramesh, Gabriel Goh, Sandhini Agarwal, Girish Sastry, Amanda Askell, Pamela Mishkin, Jack Clark, et al. "Learning transferable visual models from natural language supervision". In: *arXiv preprint arXiv:2103.00020*. 2021.
- [RR23] Elan Rosenfeld and Andrej Risteski. "Outliers with Opposing Signals Have an Out-sized Effect on Neural Network Optimization". In: *arXiv preprint arXiv:2311.04163* (2023).
- [RSG16] Marco Tulio Ribeiro, Sameer Singh, and Carlos Guestrin. "'Why should I trust you?' Explaining the predictions of any classifier". In: *International Conference on Knowledge Discovery and Data Mining (KDD)*. 2016.
- [RTG+22] Shauli Ravfogel, Michael Twiton, Yoav Goldberg, and Ryan D Cotterell. "Linear adversarial concept erasure". In: *International Conference on Machine Learning*. PMLR. 2022, pp. 18400–18421.
- [RWC+19] Alec Radford, Jeff Wu, Rewon Child, David Luan, Dario Amodei, and Ilya Sutskever. "Language Models are Unsupervised Multitask Learners". In: (2019).
- [SBS23] Alessandro Stolfo, Yonatan Belinkov, and Mrinmaya Sachan. "Understanding Arithmetic Reasoning in Language Models using Causal Mediation Analysis". In: *arXiv preprint arXiv:2305.15054* (2023).
- [SCN+19] Emily Sheng, Kai-Wei Chang, Premkumar Natarajan, and Nanyun Peng. "The woman worked as a babysitter: On biases in language generation". In: *arXiv preprint arXiv:1909.01326* (2019).
- [SJNI21] Harshay Shah, Prateek Jain, and Praneeth Netrapalli. "Do Input Gradients Highlight Discriminative Features?" In: *Advances in Neural Information Processing Systems 34* (2021).
- [SKH+20] Shiori Sagawa, Pang Wei Koh, Tatsunori B. Hashimoto, and Percy Liang. "Distributionally Robust Neural Networks for Group Shifts: On the Importance of Regularization for Worst-Case Generalization". In: *International Conference on Learning Representations*. 2020.
- [SPI+23] Harshay Shah, Sung Min Park, Andrew Ilyas, and Aleksander Madry. "Modeldiff: A framework for comparing learning algorithms". In: *International Conference on Machine Learning*. PMLR. 2023, pp. 30646–30688.
- [SRC23] Aaquib Syed, Can Rager, and Arthur Conmy. "Attribution Patching Outperforms Automated Circuit Discovery". In: *arXiv preprint arXiv:2310.10348* (2023).
- [STE+21] Shibani Santurkar, Dimitris Tsipras, Mahalaxmi Elango, David Bau, Antonio Torralba, and Aleksander Madry. "Editing a classifier by rewriting its prediction rules". In: *Preprint*. 2021.
- [STR+20] Harshay Shah, Kaustav Tamuly, Aditi Raghunathan, Prateek Jain, and Praneeth Netrapalli. "The pitfalls of simplicity bias in neural networks". In: *Advances in Neural Information Processing Systems 33* (2020), pp. 9573–9585.

- [STY17] Mukund Sundararajan, Ankur Taly, and Qiqi Yan. “Axiomatic attribution for deep networks”. In: *International Conference on Machine Learning (ICML)*. 2017.
- [SVZ13] Karen Simonyan, Andrea Vedaldi, and Andrew Zisserman. “Deep inside convolutional networks: Visualising image classification models and saliency maps”. In: *arXiv preprint arXiv:1312.6034* (2013).
- [VGB+20] Jesse Vig, Sebastian Gehrmann, Yonatan Belinkov, Sharon Qian, Daniel Nevo, Yaron Singer, and Stuart Shieber. “Investigating gender bias in language models using causal mediation analysis”. In: *Advances in neural information processing systems* 33 (2020), pp. 12388–12401.
- [VJE+23] Joshua Vendrow, Saachi Jain, Logan Engstrom, and Aleksander Madry. “Dataset interfaces: Diagnosing model failures using controllable counterfactual generation”. In: *arXiv preprint arXiv:2302.07865* (2023).
- [VSP+17] Ashish Vaswani, Noam Shazeer, Niki Parmar, Jakob Uszkoreit, Llion Jones, Aidan N Gomez, Łukasz Kaiser, and Illia Polosukhin. “Attention is All you Need”. In: *Advances in Neural Information Processing Systems* (2017).
- [WBW+11] Catherine Wah, Steve Branson, Peter Welinder, Pietro Perona, and Serge Belongie. “The caltech-ucsd birds-200-2011 dataset”. In: (2011).
- [WGX+19] Haohan Wang, Songwei Ge, Eric P Xing, and Zachary C Lipton. “Learning robust global representations by penalizing local predictive power”. In: *Neural Information Processing Systems (NeurIPS)* (2019).
- [WLL+23] Kaiyue Wen, Yuchen Li, Bingbin Liu, and Andrej Risteski. “Transformers are uninterpretable with myopic methods: a case study with bounded Dyck grammars”. In: *arXiv preprint arXiv:2312.01429* (2023).
- [WVC+22] Kevin Wang, Alexandre Variengien, Arthur Conmy, Buck Shlegeris, and Jacob Steinhardt. *Interpretability in the Wild: a Circuit for Indirect Object Identification in GPT-2 small*. 2022. DOI: [10.48550/ARXIV.2211.00593](https://doi.org/10.48550/ARXIV.2211.00593). URL: <https://arxiv.org/abs/2211.00593>.
- [WYS+23] Zhenyi Wang, Enneng Yang, Li Shen, and Heng Huang. “A comprehensive survey of forgetting in deep learning beyond continual learning”. In: *arXiv preprint arXiv:2307.09218* (2023).
- [ZF14] Matthew D Zeiler and Rob Fergus. “Visualizing and understanding convolutional networks”. In: *European conference on computer vision*. Springer. 2014, pp. 818–833.
- [ZLK+17] Bolei Zhou, Agata Lapedriza, Aditya Khosla, Aude Oliva, and Antonio Torralba. “Places: A 10 million image database for scene recognition”. In: *IEEE transactions on pattern analysis and machine intelligence*. 2017.
- [ZN23] Fred Zhang and Neel Nanda. “Towards Best Practices of Activation Patching in Language Models: Metrics and Methods”. In: *arXiv preprint arXiv:2309.16042* (2023).
- [ZPC+23] Andy Zou, Long Phan, Sarah Chen, James Campbell, Phillip Guo, Richard Ren, Alexander Pan, Xuwang Yin, Mantas Mazeika, Ann-Kathrin Dombrowski, et al. “Representation engineering: A top-down approach to ai transparency”. In: *arXiv preprint arXiv:2310.01405* (2023).
- [ZPD+23] Xiaosen Zheng, Tianyu Pang, Chao Du, Jing Jiang, and Min Lin. “Intriguing Properties of Data Attribution on Diffusion Models”. In: *arXiv preprint arXiv:2311.00500* (2023).

- [ZRZ+20] Chen Zhu, Ankit Singh Rawat, Manzil Zaheer, Srinadh Bhojanapalli, Daliang Li, Felix Yu, and Sanjiv Kumar. “Modifying memories in transformer models”. In: *arXiv preprint arXiv:2012.00363* (2020).
- [ZSB+18] Bolei Zhou, Yiyou Sun, David Bau, and Antonio Torralba. “Revisiting the importance of individual units in cnns via ablation”. In: *arXiv preprint arXiv:1806.02891* (2018).

Appendices

A	Evaluation setup	30
A.1	Pseudocode	30
A.2	Datasets and models.	30
A.3	Baselines	31
A.4	Implementation details	32
B	Applying COAR to language models	34
B.1	Evaluating GPT-2 on the TinyStories dataset	34
B.2	Evaluating Phi-2 on the BoolQ dataset	34
C	Additional evaluation of COAR	37
C.1	Evaluating COAR on additional datasets	37
C.2	Evaluating COAR on additional model architectures	37
C.3	Evaluating COAR on additional tasks	37
C.4	Comparing COAR attributions estimated with different ablation fractions	38
C.5	Comparing COAR attributions estimated with different sample sizes	38
C.6	Analyzing COAR attributions at the example level	38
C.7	Qualitatively analyzing COAR attributions	38
D	Additional evaluation of COAR-EDIT	48
D.1	Editing individual predictions	48
D.2	Forgetting a class	48
D.3	Improving subpopulation robustness.	49
D.4	Mitigating backdoor attacks.	49
D.5	Improving robustness to typographic attacks.	50
E	Analyzing design choices in COAR	57
E.1	Effect of ablation fraction	57
E.2	Effect of ablation method	57
E.3	Effect of model output function	58

A Evaluation setup

In this section, we outline the experiment setup—datasets, models, baselines, implementation details—used in Section 4 to evaluate whether COAR attributions can accurately estimate ground-truth component counterfactuals.

A.1 Pseudocode

Algorithm 1 An outline for estimating component attributions with COAR.

```
1: procedure COAR(example  $z$ , model  $M$  with output function  $f_M$  and components  $C$ , ablation
   frac.  $\alpha$ )
2:   Set  $D^{(z)} \leftarrow []$   $\triangleright$  initialize component dataset (2)
3:   for  $i \in \{1, \dots, m\}$  do  $\triangleright m$  denotes dataset size
4:     Sample a subset  $C_i \subset C$  from  $\mathcal{D}_C$  where  $|C_i| = \alpha \cdot |C|$ 
5:     Set  $y_i \leftarrow f_M(z, C_i)$   $\triangleright$  compute component counterfactual (1)
6:     Define  $\mathbf{0}_{C_i} \in \{0, 1\}^{|C|}$  as  $(\mathbf{0}_{C_i})_j = 0$  if  $c_j \in C_i$  else 1
7:     Update  $D^{(z)} \leftarrow D^{(z)} + [(\mathbf{0}_{C_i}, y_i)]$   $\triangleright$  update component dataset
8:    $\theta^{(z)}, b^{(z)} \leftarrow \text{LINEARREGRESSION}(D^{(z)})$   $\triangleright$  estimate component attributions via Equation 3
9:   return  $\theta^{(z)}, b^{(z)}$ 
```

A.2 Datasets and models.

We now outline the datasets and models used to evaluate COAR (§4) and COAR-EDIT (§5).

CIFAR-10. We use the standard CIFAR-10 [Kri09] image classification dataset to evaluate COAR attributions (Section 4, Appendix C.2) and for an editing task (Section 5.4). We train ResNet, ViT, and MLP models that attain test accuracies of 91%, 83% and 56% respectively. We specify a computation graph over 2,344 components for the ResNet-18 model, 31,728 components for the ViT model, and 3,072 components for the MLP model. Each component in the ResNet-18 model corresponds to a convolution filter. Similarly, each component in the ViT and MLP models corresponds to a neuron.

ImageNet. We use the standard ImageNet [DDS+09] image classification dataset to evaluate COAR attributions in Section 4 and for editing tasks in Section 5.2. We use ImageNet-Sketch [WGX+19] and five random shifts from ImageNet* [VJE+23]—“in the water”, “at dusk simple”, “orange”, “pencil sketch”, “green”—to evaluate the out-of-distribution performance of edited ImageNet models in Section 5.2. We use the pre-trained ResNet50 and ViT-B/16 models² that attain test accuracies of 75.4% and 80.7% respectively. For the ResNet-50 model, we specify a computation graph over 22,720 components, each corresponding to a convolution filter. Similarly, for the ViT-B/16 model, we specify a computation graph over 82,944 components, each corresponding to a neuron.

²Model and pre-trained weights taken from torchvision: <https://pytorch.org/vision/stable/models.html>

Waterbirds. The Waterbirds dataset [SKH+20] comprises images of birds taken from the CUB dataset [WBW+11] and pasted on backgrounds from the Places dataset [ZLK+17]. The task here is to classify “waterbirds” and “landbirds” in the presence of spurious correlated “land” and “water” backgrounds in the training dataset. Sagawa et al. [SKH+20] introduce Waterbirds as a benchmark to improve model performance under subpopulation shifts induced by spurious correlations. We use this dataset to evaluate whether COAR-EDIT can improve subpopulation robustness via model editing. In this experiment, we fine-tune an ImageNet ResNet50 model and use a computation graph over 22,720 components, each corresponding to a convolution filter.

CelebA. The CelebA dataset [LYS+20] comprises images of celebrities with binary attributes such as “smiling”, “wearing hat”, “wearing lipstick”, etc. Similar to previous work on subpopulation robustness (e.g., [SKH+20]), we repurpose CelebA as a binary classification task where the goal is to predict whether a person in a given image has blond hair. The attributes “hair color” and “gender” are spuriously correlated in the training dataset, resulting in models that latch on to a “gender \rightarrow blond hair” shortcut and underperform on the “blond males” subpopulation. Similar to the Waterbirds setting, we fine-tune an ImageNet ResNet50 model and specify a computation graph over 22,720 components, each corresponding to a convolution filter.

Typographic attacks dataset. We use a dataset of typographic attacks [MTB22] for an editing task in Section 5.5. This dataset comprises 180 images of household objects with and without eight typographic attacks such as “taxi”, “twitter”, “EU”, and “iPad”. We visualize some examples from this dataset in Figure 7. Our experiment in Section 5.5 uses this dataset along with a zero-shot CLIP ViT-B/16 classifier [RKH+21]. For this model, we specify a computation graph over all 82,944 components, corresponding to the set of all weight vectors (individual rows in weight matrices) in all self-attention and MLP modules. See Appendix D.5 for more details.

TinyStories. We use the TinyStories dataset [EL23] to evaluate COAR attributions over the GPT-2 language model (Appendix B). This dataset contains short stories synthetically generated by GPT-3.5 and GPT-4. To compute component attributions for GPT-2, we specify a computation graph over 64,512 components, which correspond to the set of all weight vectors, i.e., in every self-attention module and feed-forward module of the model. See Appendix B.1 for experiment details and findings.

BoolQ. We use the BoolQ dataset [CLC+19] to evaluate COAR attributions for the Phi-2 model [LBE+23]. Each example in this dataset comprises a passage of text, a question, and a binary answer. We evaluate the zero-shot performance of Phi-2 using the prompting and evaluation procedure from Gao et al. [GTA+23]³. Given the size of the Phi-2 model, we specify a computation graph over 55,552 components, each corresponding to a contiguous block of 10 weight vectors in every self-attention module and feed-forward module of the model. See Appendix B.2 for experiment details and findings.

A.3 Baselines

In Section 4, we compare COAR against four baseline methods for estimating component attributions: Leave-One-Out (LOO), Gradient-times-parameters (GP), Neuron Conductance (NC), and Internal Influence (II). Each baseline computes an attribution vector $w^{(z)} \in \mathbb{R}^{|C|}$ for a given example

³<https://github.com/EleutherAI/lm-evaluation-harness/>

z by assigning an “importance” score $w_j^{(z)}$ to each component $c_j \in C$. Then, as per Equation 4, we estimate a component counterfactual $f_M(z, C')$ as the sum of importance scores of components in $C \setminus C'$, i.e., scores of components that are not ablated. We describe each baseline in more detail below:

- **Leave-One-Out (L00)**: This method ablates each component $c_j \in C$ and sets the coefficient $\theta^{(z)}_j$ to the change in model output $f_M(z)$ before and after ablation:

$$w_j^{(z)} = f_M(z, \{c_j\}) - f_M(z, \emptyset)$$

- **Gradient-times-Parameters (GP)**: This method approximates the leave-one-out estimate described above. Specifically, it estimates the leave-one-out effect of each component $c_j \in C$ using a first-order Taylor approximation of $f_M(z, \{c_j\})$ around $f_M(z, \emptyset)$:

$$w_j^{(z)} = \nabla_{c_j} f_M(z, \emptyset) \cdot \delta_{c_j}$$

where δ_{c_j} is the parameter-space change in c_j induced by the ablation method of choice.

- **Neuron Conductance (NC)** [DSY18]: This method extends the Integrated Gradients method [STY17]—an input-space feature attribution method—to compute importance scores for each component $c_j \in C$. Intuitively, NC modifies the computation in Integrated Gradients in order to quantify the “flow” through each component $c_j \in C$. See Equation 3 in [DSY18] for a formal description.
- **Internal Influence (II)** [LSD+18]: Similar to NC, this method also adapts Integrated Gradients [STY17] to compute importance scores. At a high level, II directly applies Integrated Gradients to layerwise activations by treating the output of each layer as an input to subsequent layers. See Definition 1 in [LSD+18] for a formal description.

We implement the first two baselines (L00 and GP) from scratch⁴ and use the captum library [KMM+20]⁵ to implement NC and II. As per Definition 2, we estimate the component counterfactual $f_M(z, C')$ using these baselines by setting the bias term $b^{(z)}$ to zero and taking the sum over attribution scores of components that are not ablated.

A.4 Implementation details

Sample size for component attribution estimation. The computational cost of our approach linearly scales with the sample size m used to estimate component attributions (see Algorithm 1). Each sample in the component dataset $D^{(z)}$ corresponds to a single forward pass through the model M in order to compute the counterfactual $f_M(z, C')$ (1), i.e., model output $f_M(z)$ after ablating a subset of components $C' \subset C$. The setups $\{A, B, C\}$ considered in Section 4 use sample size $m = \{50000, 100000, 200000\}$ respectively. In Appendix C.5, we show that the sample size m used in Section 4 can be reduced by 2-5 \times , resulting in a direct speedup while only reducing the predictive power of COAR attributions by a small amount.

Data loading. We use the FFCV library⁶ [LIE+22] to train and evaluate models. FFCV removes the data loading bottleneck for small models, gives a 3-4 \times improvement in throughput compared to standard PyTorch data loading.

⁴Our code is available at <https://github.com/MadryLab/modelcomponents>

⁵Github repository: <https://github.com/pytorch/captum>

⁶Github repository: <https://github.com/libffcv/ffcv>

Speeding up regression. The second step of COAR—fitting component attributions to the component dataset (2)—requires solving a linear regression problem (Equation 3) for each example z . We parallelize this step by using the `fast-11` package⁷, a SAGA-based GPU solver for linear regression.

Computing resources. We train our models and compute COAR attributions on a cluster of machines, each with 9 NVIDIA A100 or V100 GPUs and 96 CPU cores. We also use half-precision to increase training speed.

⁷Github repository: https://github.com/MadryLab/fast_11

B Applying COAR to language models

In Section 4 and Appendix C, we showed that our proposed method COAR attributions accurately estimate component counterfactuals (1) on large-scale vision tasks across several datasets and model architectures. In this section, we apply COAR to language models. Specifically, we consider two experiments: (a) GPT-2 [RWC+19] evaluated on the next-token prediction task and (b) Phi-2 [LBE+23] evaluated on a zero-shot classification task. In both cases, we show that COAR attributions accurately predict how model outputs change in response to component ablations.

B.1 Evaluating GPT-2 on the TinyStories dataset

Task and model output function. We apply COAR to the next-token prediction task. Following Park et al. [PGI+23], we interpret this task as a sequence as a v -way classification problem, where v is the vocabulary size, and set the model output function to be the average correct-class margin (5) over all tokens in a given sequence.

Model and dataset. In this experiment, we consider the GPT-2 model⁸ [RWC+19], with a computation graph over 64,512 components. These components correspond to the set of weight vectors in every self-attention module and feed-forward module in the model. We evaluate model performance on the next-token prediction task using the TinyStories dataset⁹ [EL23], where each sequence corresponds to a synthetically generated short story.

Computing COAR attributions. We apply COAR (without any modifications) to compute component attributions for a random subset of 1000 examples in the TinyStories validation set using a component dataset of 200,000 component counterfactuals (2) and a ablation fraction of $\alpha = 2.5\%$.

Evaluating COAR attributions. Similar to the results in Section 4, COAR attributions are predictive in the language modeling setting as well. Specifically, these attributions accurately predict the effect of ablating components on the average correct-class margin of GPT-2 on examples from the TinyStories validation set. In Figure 8a, we pick a random example z from the TinyStories validation set and compute the correlation between ground-truth component counterfactuals $f_M(z, \cdot)$ and the corresponding estimate (4) using its COAR attributions $\theta^{(z)}$, as defined in Equation 6. In Figure 8b, we plot a histogram over example-level correlations of 1000 examples and find that COAR attributions attain an average correlation of $\{0.83, 0.85, 0.89\}$ with ground-truth component counterfactuals sampled using ablation fraction $\alpha = \{5\%, 2.5\%, 1\%\}$ respectively.

B.2 Evaluating Phi-2 on the BoolQ dataset

Task and model output function. We now turn to a reading comprehension task, where the goal is to answer a question given a passage of text. We evaluate this classification task in a zero-shot manner: the language model is prompted with a passage of text and a question, and the goal is to output the correct answer from {yes, no}. Like in vision tasks (Section 4), we use the correct-class margin (5) as the model output function for this zero-shot binary classification task.

⁸<https://huggingface.co/gpt2>

⁹<https://huggingface.co/datasets/roneneldan/TinyStories>

Model and dataset. We consider the Phi-2 model¹⁰ [LBE+23] and specify a computation graph over 55,552 components. Here, each component corresponds to a contiguous block of 10 weight vectors in the model. We evaluate this model on the BoolQ dataset¹¹ [CLC+19], where each example consists of a passage of text, a question, and a binary {yes, no} answer. Using the prompting and evaluation procedure from the Gao et al. [GTA+23]¹², Phi-2 attains an 83.6% accuracy on this task.

Computing COAR attributions. Like in Appendix B.1, we apply compute COAR attributions for a random subset of 500 examples in the BoolQ validation set using a component dataset of $m = 100,000$ component counterfactuals (2) and a ablation fraction of $\alpha = 0.025$.

Evaluating COAR attributions. We find that COAR attributions are predictive of unseen component counterfactuals on this task as well. Figure 9a plots the correlation between ground-truth component counterfactuals $f_M(z, \cdot)$ and the corresponding COAR estimate (4) of a random BoolQ example z . The histograms in Figure 9b show that COAR attributions attain an average correlation of $\{0.58, 0.66, 0.66\}$ with ground-truth component counterfactuals sampled using ablation fraction $\alpha = \{5\%, 2.5\%, 1\%\}$ respectively.

¹⁰<https://huggingface.co/microsoft/phi-2>

¹¹<https://huggingface.co/datasets/google/boolq>

¹²<https://github.com/EleutherAI/lm-evaluation-harness>

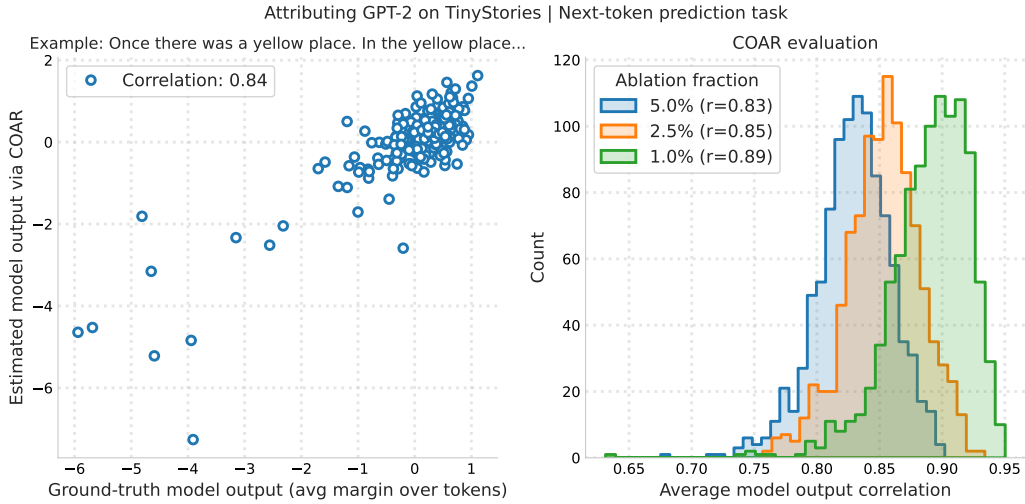


Figure 8: **Evaluating COAR on GPT-2.** We apply COAR to the GPT-2 model [RWC+19] on the TinyStories dataset [EL23]. The resulting component attributions are predictive of component counterfactuals. The left plot shows that component attributions can estimate the effect of ablating components on the average correct-class margin (over tokens in a sequence) of GPT-2 on a random TinyStories example with high correlation. The histograms in the right plot show that COAR attributions attain high average correlation for multiple values of ablation fraction α .

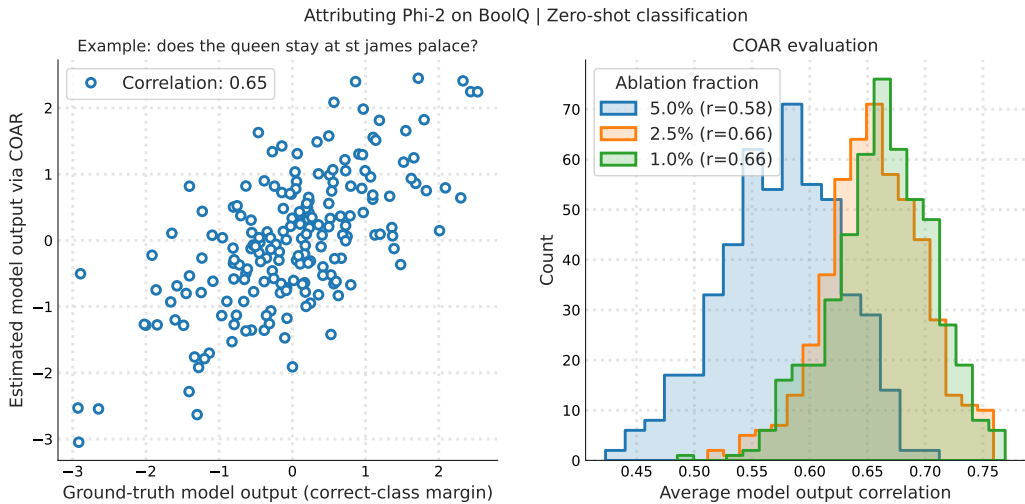


Figure 9: **Evaluating COAR on Phi-2.** We apply COAR to the Phi-2 model [JB23] on the BoolQ dataset [CLC+19]. The resulting component attributions are predictive of component counterfactuals. The left plot shows that component attributions can estimate the effect of ablating components on the average correct-class margin of Phi-2 on a random BoolQ example with high correlation. The histograms in the right plot show that COAR attributions attain high average correlation for multiple values of ablation fraction α .

C Additional evaluation of COAR

In this section, we first show that COAR learns accurate component attributions on additional datasets, model architectures, and tasks (Appendices C.1 to C.3). This supplements our findings in Section 4, where we showed that COAR learns component attributions that accurately predict component counterfactuals (1) on three image classification setups: CIFAR-10 ResNet-18, ImageNet ResNet-50, and ImageNet ViT-B/16. Then, we show that COAR attributions retain its predictive power when estimated with fewer samples (Appendix C.5) or with different ablation fractions (Appendix C.4). Finally, we supplement our example-level evaluation of COAR attributions in Section 4 with additional example-level comparisons of ground-truth component counterfactuals and attribution-based estimates (Appendix C.6).

C.1 Evaluating COAR on additional datasets

Our experiments in Section 4 evaluated the predictiveness of COAR attributions corresponding to in-distribution test examples from the CIFAR-10 and ImageNet datasets. Now, we show that COAR attributions remain predictive on training examples as well as out-of-distribution examples. Specifically, we apply COAR to compute attributions of ResNet-18 predictions on the CIFAR-10 training set and on six corrupted versions of the CIFAR-10 test set [HD19]. as shown in Figure 10, COAR attributions exhibit high correlation on average (between 0.6 and 0.8) depending on the ablation fraction α used to ablate random α -fraction sized components subsets. Note that the correlation is maximum when $\alpha = 0.05$ because the component attributions are estimated with the same ablation fraction, i.e., $\alpha_{\text{train}} = 0.05$.

C.2 Evaluating COAR on additional model architectures

Recall that COAR is model-agnostic in that it is not tied to any specific model architecture. In Section 4, we applied COAR to ResNets trained on CIFAR-10 and ImageNet and a ViT-B/16 model trained on ImageNet. In this section, we apply COAR to two additional model architectures: a ViT model trained on CIFAR-10 (83% accuracy) and a one-layer fully-connected network trained on CIFAR-10 (56% accuracy). Figure 11 shows that COAR attributions on both architectures yield accurate estimates of how model outputs change in response to ablating random α -fraction sized components subsets, with correlation 0.65 and 0.85 for the ViT and MLP models when $\alpha = \alpha_{\text{train}}$ respectively.

C.3 Evaluating COAR on additional tasks

We now evaluate COAR attributions on four additional tasks:

- First, we apply COAR to pre-trained ImageNet ResNet50 model fine-tuned on two datasets—Waterbirds and CelebA—that we use in Section 5.3—see first row of Figure 12. We find that COAR attributions are predictive on both datasets, attaining higher correlation with ground-truth component counterfactuals when α is closer to $\alpha_{\text{train}} = 0.05$.
- Second, we apply COAR to a pre-trained ImageNet ResNet50 model fine-tuned on MIMIC-CXR [JPG+19], a dataset of labeled chest radiographs. In this case, we set the model output function to be the logit of the “Cardiomegaly” class instead of correct-class margin that we use in Section 4. Figure 12 shows that COAR attributions attain a correlation of 0.7 and 0.6 with ground-truth logits when $\alpha = \alpha_{\text{train}} = 0.05$ and $\alpha = 0.10$ respectively.

- The fourth plot in Figure 12 corresponds to the CLIP setting considered in Section 5. In this setting, we take the zero-shot CLIP ViT-B/16 classifier and evaluate it on a dataset of images with and without typographic attacks [MTB22]. As shown in the plot, the correlation between COAR attributions and ground-truth margins is close to 0.7 when $\alpha = \alpha_{\text{train}} = 0.03$, i.e., ablating 3% of the components in the CLIP model.

C.4 Comparing COAR attributions estimated with different ablation fractions

We now analyze how changing the ablation fraction α_{train} used to fit COAR attributions affects their predictiveness over different ablation fractions at test time. Specifically, we consider the ImageNet ResNet-50 setting from Section 4 and compute two sets of COAR attributions, corresponding to two values of α_{train} : 0.05 and 0.10. Then, for each of these two sets of attributions, we evaluate its correlation with ground-truth component counterfactuals over a range of ablation fractions α . As shown in Figure 13, the correlation “profile” over α depends on the value of α_{train} used to fit the attributions. When α is small, the correlation is higher for attributions estimated with $\alpha_{\text{train}} = 0.05$. Analogously, when α is large, the correlation is higher for attributions estimated with $\alpha_{\text{train}} = 0.10$. This is because the component attributions fare better as counterfactual predictors on component counterfactuals that are “similar” to the ones used to fit them—i.e., when $\alpha_{\text{test}} \approx \alpha_{\text{train}}$.

C.5 Comparing COAR attributions estimated with different sample sizes

In Section 4, we computed COAR attributions using sample sizes $m = 50000$ for the ResNet-18 model trained on CIFAR-10 and $m = 100000$ for the ResNet-50 model trained on ImageNet. Recall that the sample size m here corresponds to the number of component counterfactuals used to fit the component attributions. In this section, we vary the sample size m and show that COAR attributions remain predictive even when trained on $k \times$ fewer examples, where $k \in \{2, 5, 10\}$. Specifically, the left column of Figure 14 shows that COAR attributions estimated on CIFAR-10 and ImageNet data with sample size m and m/k have high cosine similarity on average, with the similarity increasing as k decreases. The right column of Figure 14 shows that decreasing the sample size m by a factor of $k \in \{2, 5, 10\}$ does not significantly impact the correlation between COAR attributions and ground-truth component counterfactuals. For example, reducing the sample size by $5 \times$ only reduces the correlation from 0.7 to 0.65 in the CIFAR-10 ResNet-18 setting. Additionally, we observe that COAR attributions fare better than attributions estimated with the best-performing baseline (L00) even when trained on $10 \times$ fewer examples on CIFAR-10 and $5 \times$ fewer examples on ImageNet.

C.6 Analyzing COAR attributions at the example level

To supplement our evaluation in Section 4, we provide additional example-level scatterplot comparisons between ground-truth component counterfactuals and the corresponding estimates obtained using component attributions estimated with COAR and all baselines from Section 4. We plot these comparisons on CIFAR-10 examples in Figure 15 and on ImageNet examples in Figure 16. Our findings further substantiate that COAR attributions exhibit higher correlation with ground-truth component counterfactuals than all four baseliens on both CIFAR-10 and ImageNet.

C.7 Qualitatively analyzing COAR attributions

We qualitatively analyze COAR attributions using two visualization techniques:

Visualizing component-specific attributions across examples. Given examples $\{z_1, \dots, z_n\}$ with corresponding component attributions $\{\theta^{(z_1)}, \dots, \theta^{(z_n)}\}$, we analyze how the attribution estimates of individual components vary across the set of examples. Specifically, for a component $c_i \in C$, we visualize the examples with the most positive attribution values $\theta_i^{(z)}$ for component c_i . In this experiment, we visualize a random subset of components from the ImageNet ResNet-50 model (setup B in Section 4). As shown in Figure 17, the examples with the most positive attributions for a given component exhibit high visual similarity at different levels of granularity:

- The first, third and fifth row in Figure 17 show that the examples with the most positive attributions for `layer4.0.conv3[477]` and `layer4.2.conv3[53]` contain purple flowers, watch faces, and glass-shaped objects respectively.
- However, consistent with recent work on superposition in deep networks [EHO+22], we observe that some components such as `layer4.2.conv2[336]` in the second row as well as `layer3.1.conv3[655]` in the last row can surface dissimilar subsets of examples and do not readily map to a single semantic concept.

Visualizing nearest neighbors in attribution space. We also use component attributions as feature embeddings in order to visualize the nearest neighbors of a given example in “component attribution” space. Intuitively, this technique allows us to identify examples on which model outputs change similarly in response to component ablations. In this experiment, we visualize a random subset of examples from the CelebA dataset along with their 5 nearest neighbors using COAR attributions of a fine-tuned ImageNet ResNet-50 model. Figure 18 shows that the nearest neighbors of a given example in attribution space high visual similarity, i.e., similar facial attributes such as background (first row), hair color (second and fourth row), accessories (third row), or even the same person in different poses (last row).

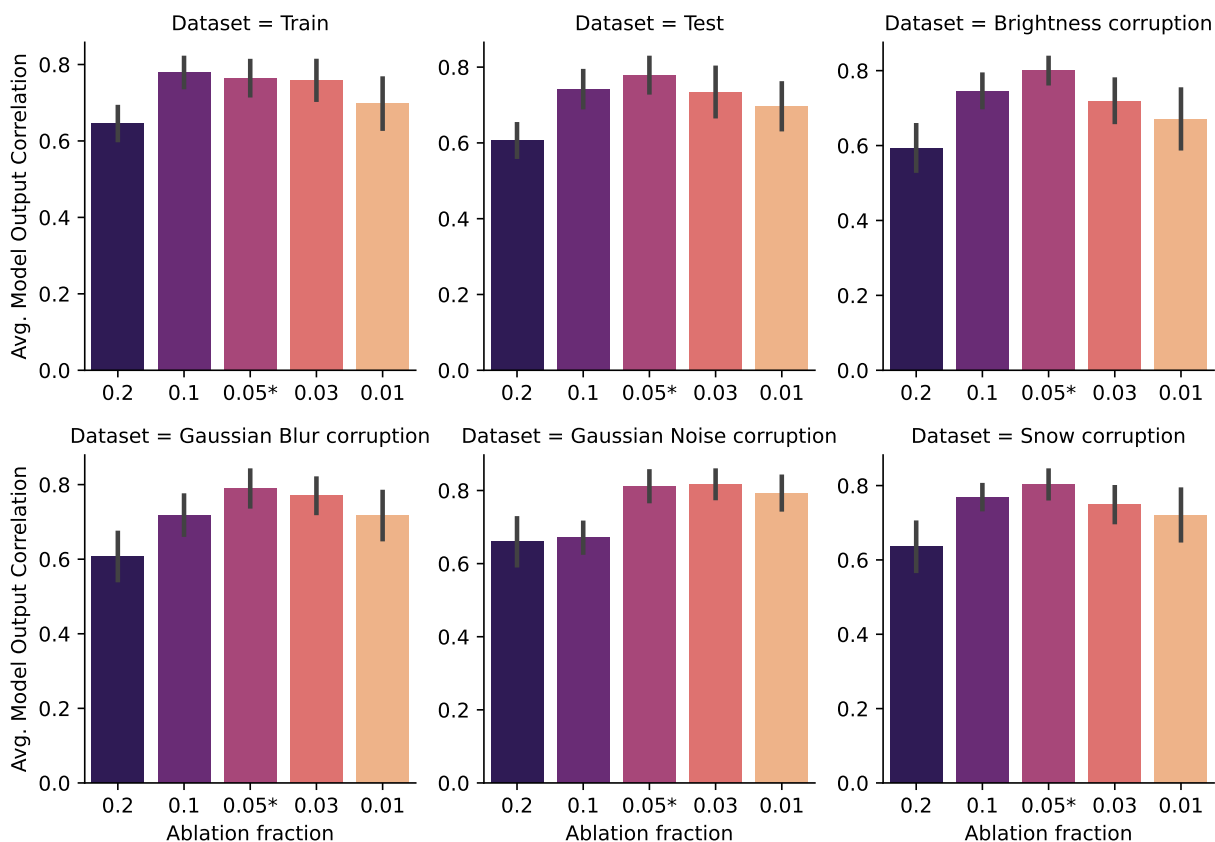


Figure 10: **Do COAR attributions generalize to out-of-distribution examples?** COAR attributions remain predictive on the CIFAR-10 training set and on six corrupted versions of the CIFAR-10 test set [HD19] over a range of ablation fractions α . See Appendix C.1 for more details.

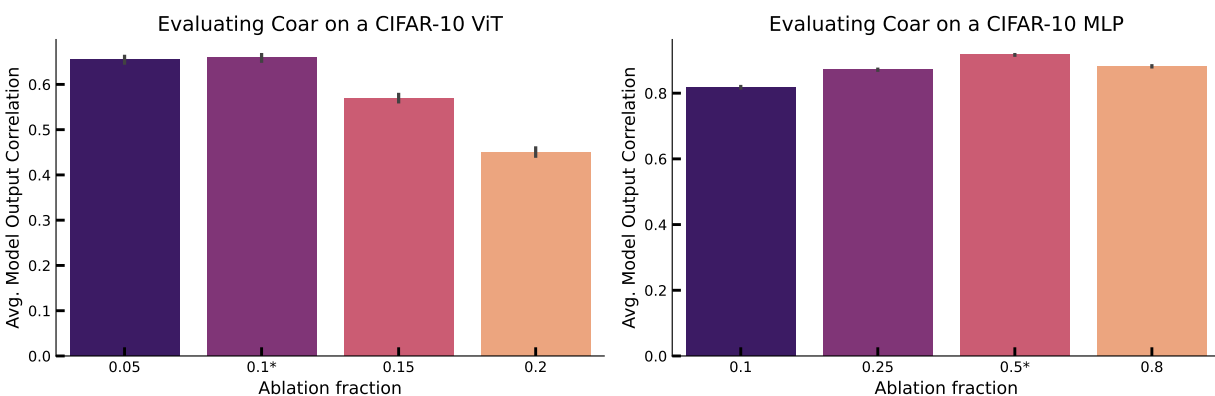


Figure 11: **Do COAR attributions generalize to other model architectures?** COAR attributions yield accurate estimates of component counterfactuals on two additional model architectures: a ViT-based model (left) and a one-layer fully-connected network (right) trained on CIFAR-10. See Appendix C.2 for more details.

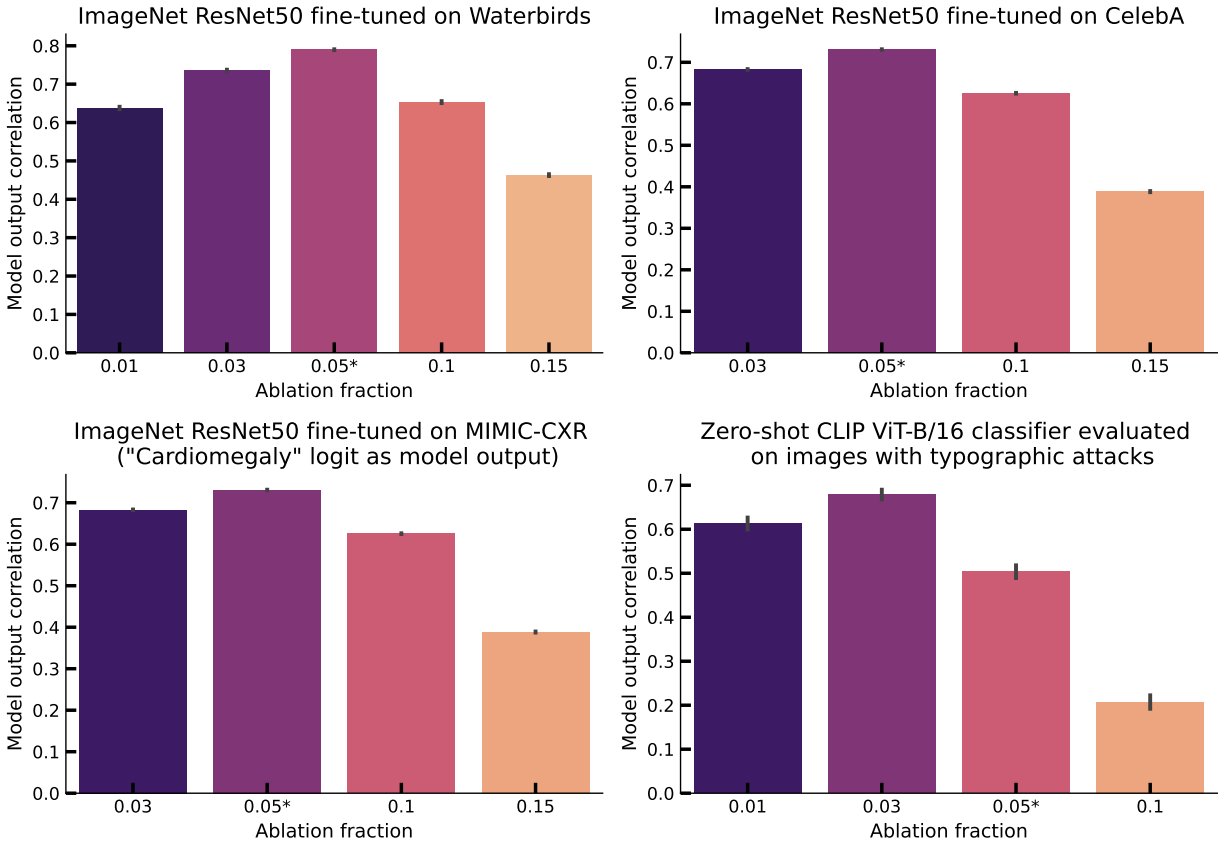


Figure 12: **Evaluating COAR attributions on additional tasks.** We find that component attributions estimated using COAR are predictive on four additional tasks: fine-tuning ImageNet ResNet50 on Waterbirds, CelebA and MIMIC-CXR, and a zero-shot CLIP ViT-B/16 classification task on a dataset containing typographic attacks (Section 5.5). Note that the MIMIC-CXR setting uses the logit of the “Cardiomegaly” class as the model output function. See Appendix C.3 for additional information about these tasks.

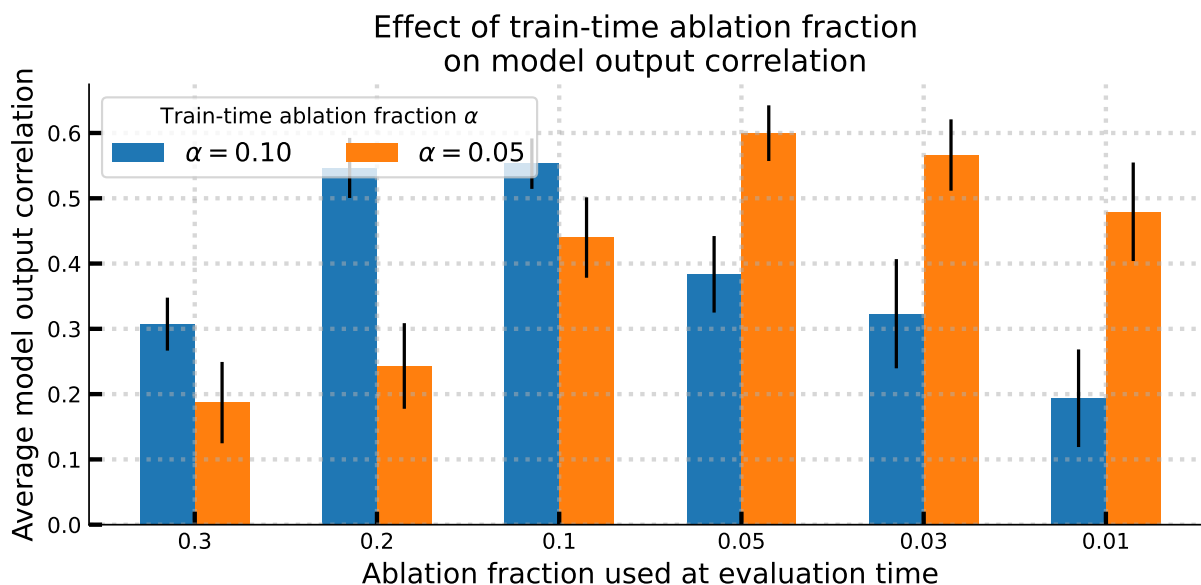


Figure 13: **Comparing COAR attributions estimated with different ablation fractions α .** COAR attributions estimated with different ablation fractions α_{train} attain a different correlation “profile” over α at test time. The correlation between ground-truth component counterfactuals and attribution-based estimates is higher for attributions estimated with $\alpha_{\text{train}} = 0.05$ when α is small, and higher for attributions estimated with $\alpha_{\text{train}} = 0.10$ when α is large. This empirically shows that COAR attributions are more predictive on component counterfactuals that are “similar” to the ones used to fit them—i.e., when $\alpha_{\text{test}} \approx \alpha_{\text{train}}$. See Appendix C.4 for more details.

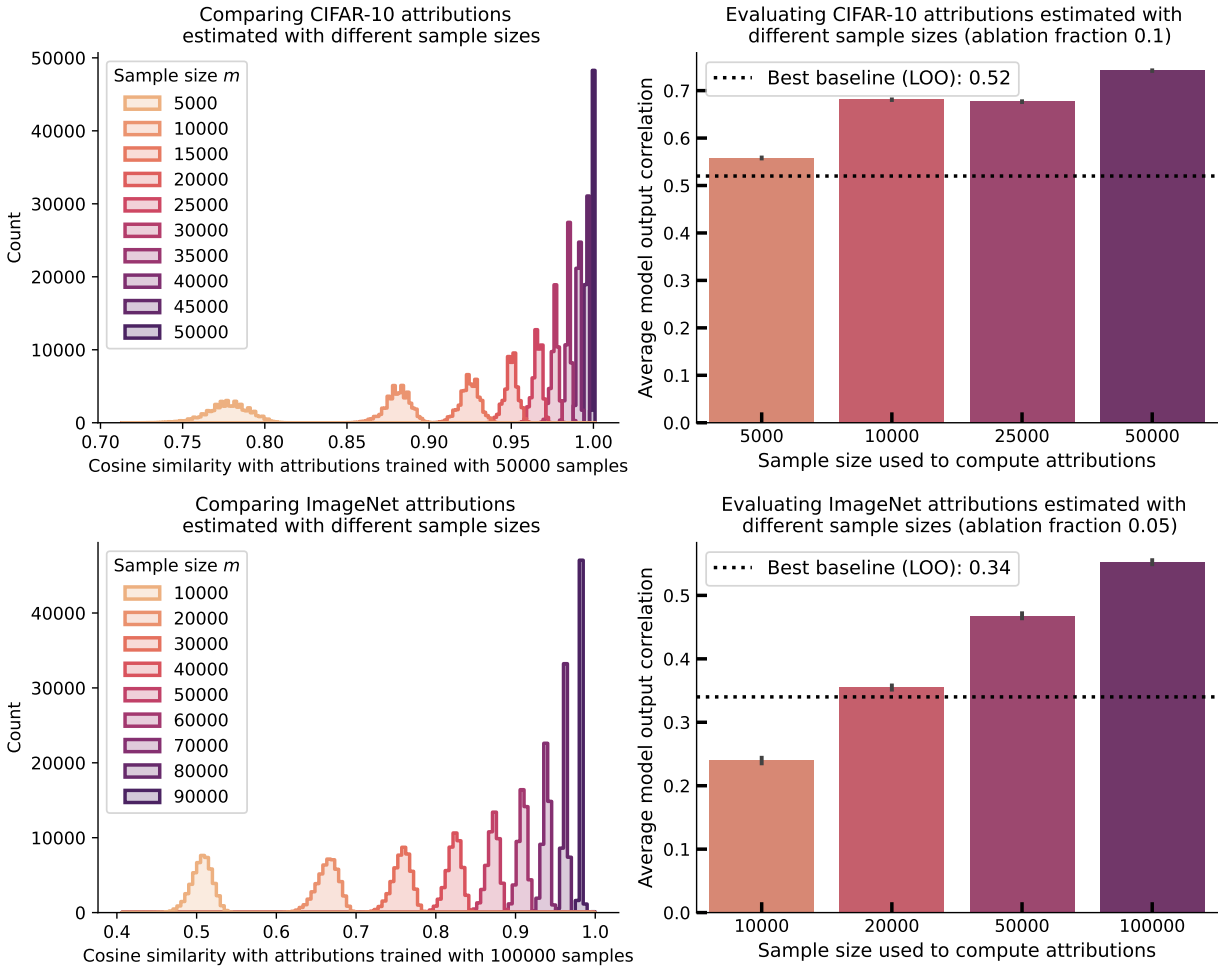


Figure 14: **Comparing COAR attributions estimated with different sample sizes.** COAR attributions for CIFAR-10 ResNet-18 and ImageNet ResNet-50 (Setup A and B respectively in Section 4) estimated with smaller sample sizes m are still predictive of component counterfactuals. On the left, we show that COAR attributions estimated with sample size m and m/k have high cosine similarity on average, with the similarity increasing as k decreases. On the right, we show that decreasing the sample size m by a factor of $k \in \{2, 5, 10\}$ does not significantly affect the correlation between COAR attributions and ground-truth component counterfactuals. In particular, COAR outperforms the best-performing baseline (LOO) even with $10\times$ fewer samples on CIFAR-10 (top row) and $5\times$ fewer samples on ImageNet (bottom row).

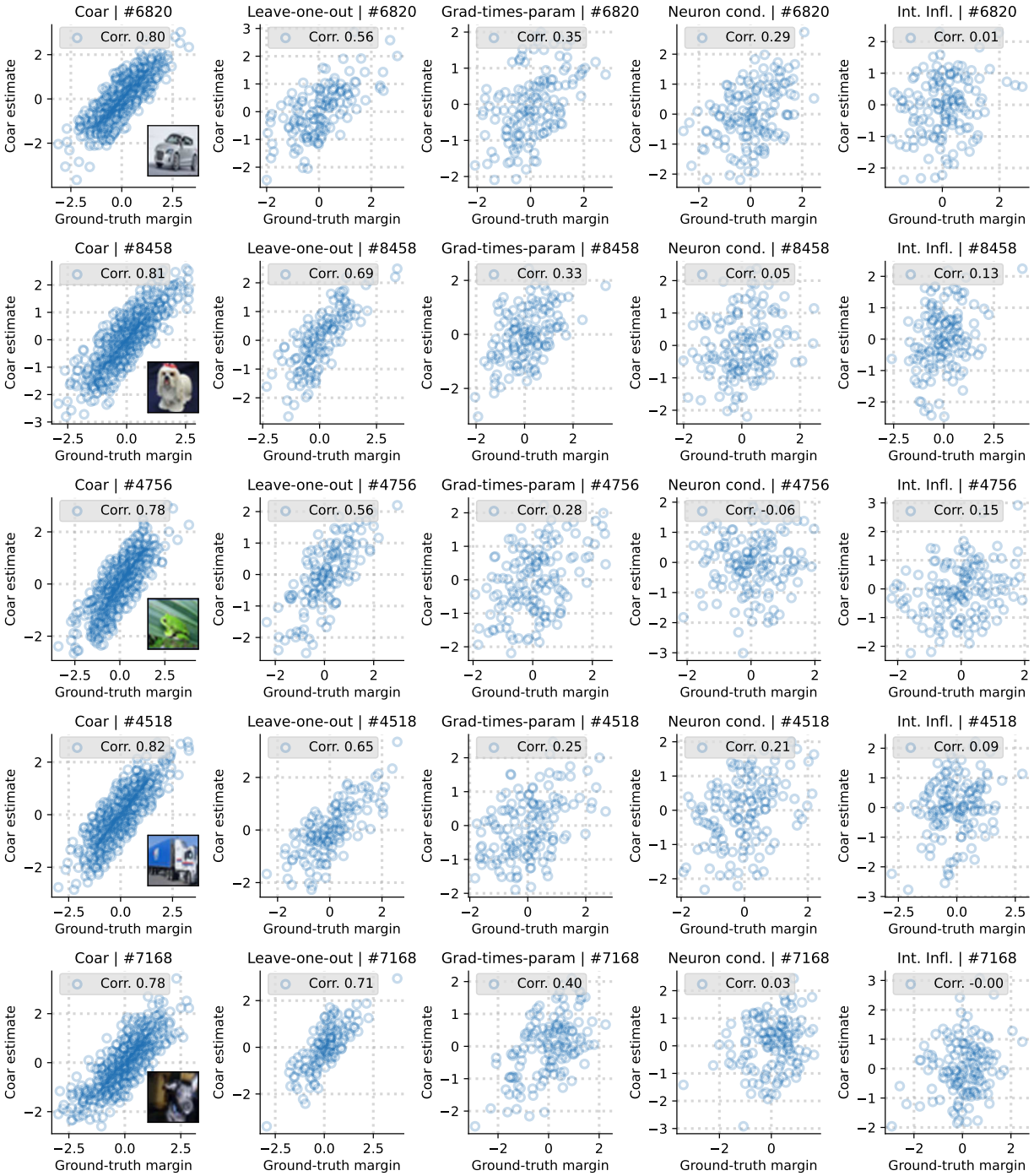


Figure 15: **Additional example-level evaluation of component attributions on CIFAR-10.** Each row corresponds to a different example z randomly picked from the CIFAR-10 test set and each column corresponds to a different attribution method. The left-most subfigure in each row shows that COAR attributions and the corresponding ground-truth component counterfactuals exhibit high correlation on example z . In comparison, the other subfigures in each row, one for baseline method, consistently exhibit lower correlation. See Appendix C.5 for more details.

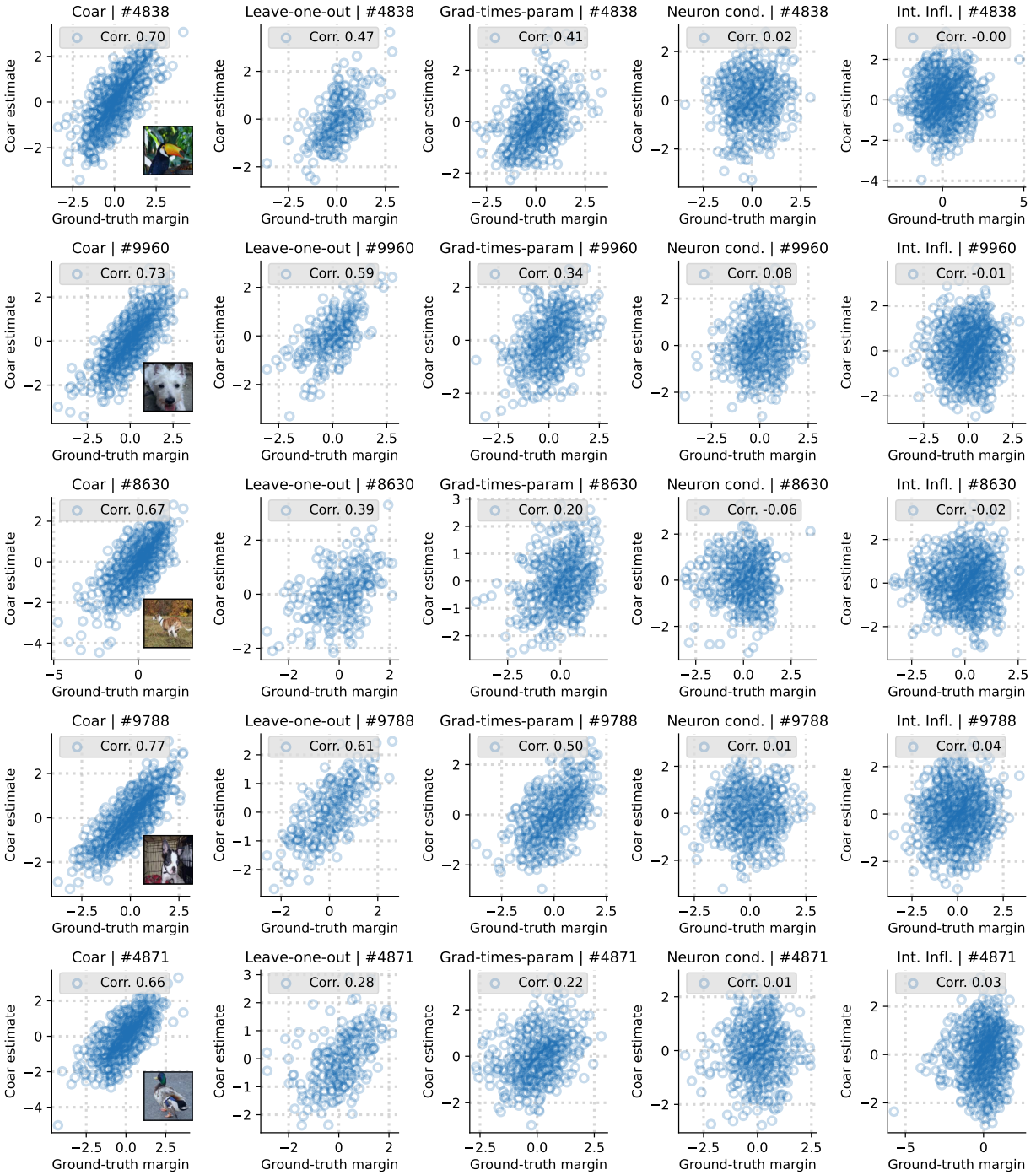


Figure 16: **Additional example-level evaluation of component attributions on ImageNet.** Similar to the results in Figure 15, each row corresponds to a different example z randomly picked from the ImageNet test set. The left-most subfigure in each row shows that COAR attributions and the corresponding ground-truth component counterfactuals exhibit high correlation on example z . In comparison, the other subfigures in each row, corresponding to a baseline method, consistently exhibit worse correlation. See Appendix C.5 for more details.

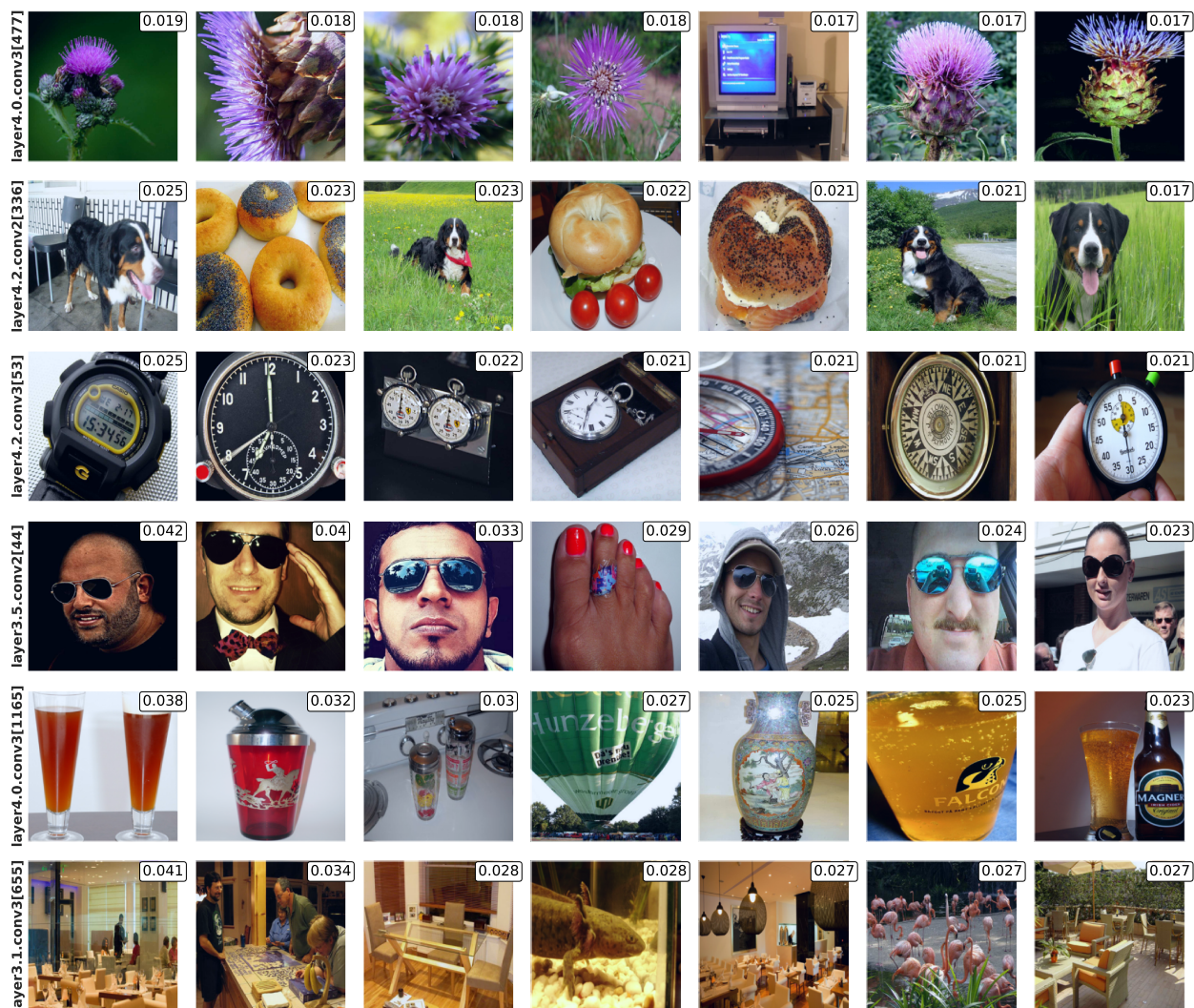


Figure 17: **Visualizing component-specific attributions across examples.** We sample a random set of components from the ImageNet ResNet-50 model (setup B in Section 4) and visualize the examples with the most positive attributions for each component. In general, the examples with the most positive attributions for a given component exhibit visual similarity at different levels of granularity. For example, the first, third and fifth row in Figure 17 show that the examples with the most positive attributions for `layer4.0.conv3[477]` and `layer4.2.conv3[53]` contain purple flowers, watch faces, and glass-shaped objects respectively. However, consistent with recent work on superposition in deep networks [EHO+22], we observe that some components such as `layer4.2.conv2[336]` (second row) and `layer3.1.conv3[655]` (last row) can surface dissimilar subsets of examples or do not readily map to a single semantic concept.

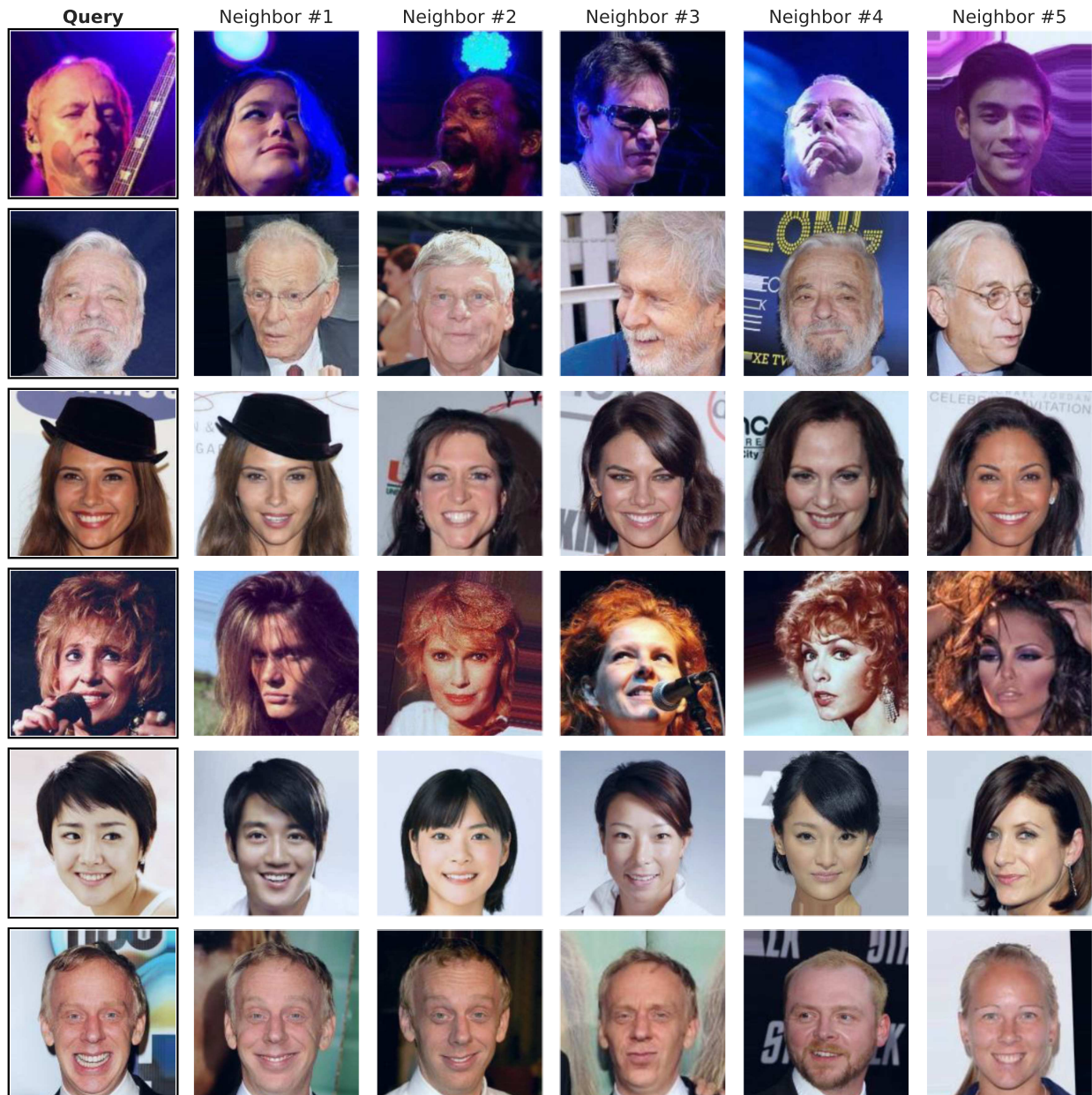


Figure 18: **Visualizing nearest neighbors in COAR attribution space.** We also use component attributions as feature embeddings in order to visualize the five nearest neighbors of examples from the CelebA dataset in “component attribution” space. Intuitively, this technique allows us to identify examples on which model outputs change similarly in response to component ablations. In general, we observe that the nearest neighbors of a given example in attribution space high visual similarity, e.g, similar facial attributes such as background (first row), hair color (second and fourth row), accessories (third row), or even the same person in different poses (last row).

D Additional evaluation of COAR-EDIT

We use COAR-EDIT in five different editing tasks: correcting misclassifications (§5.1); forgetting a class (§5.2); improving subpopulation robustness (§5.3); localizing backdoor attacks (§5.4); and improving robustness to typographic attacks (§5.5). In this section, we provide additional details and/or supplementary experiments for each task.

D.1 Editing individual predictions

Experiment details. In Section 5.1, we use COAR-EDIT to correct misclassifications of a ResNet-50 model on ImageNet examples. In this experiment, we set the “target” example to be a misclassified ImageNet example and the “reference” example to a set of 50 randomly selected ImageNet examples. Then, we use these examples to identify and ablate components (9) that increase the correct-class margin (5) of the target example without impacting the average margin over the reference examples.

Additional experiments. We first show that COAR-EDIT is not sensitive to the choice of misclassified examples, model, or dataset. In Figure 20, we reproduce the experiment in Section 5.1 on additional ImageNet examples misclassified by a ResNet-50 model. In Figure 19, we use COAR-EDIT to similarly fix misclassifications of a ResNet-18 model on the CIFAR-10 dataset. In Figure 21, we show that COAR-EDIT can also be used to adversarially induce misclassifications on ImageNet examples by ablating the top- k components corresponding to the “target” example. Similar to our findings in Section 5.1, we observe that ablating a few components via COAR-EDIT is sufficient to change the individual example-level prediction without changing overall model performance.

Additional analysis. Which components does COAR-EDIT ablate to correct misclassifications? To answer this question, we first aggregate all components ablated by COAR-EDIT in order to (individually) correct ImageNet examples misclassified by a ResNet-50 model. Then, we plot the most common convolution layers corresponding to these ablated components in Figure 22. We find that COAR-EDIT primarily targets convolution filters from the last few layers (closest to the output) of the ResNet-50 model in order to make fine-grained edits that do not impact overall model performance. For example, more than 25% of the ablated components belong to `layer4.conv3`—the last convolution layer in the first three residual blocks of the last layer group of the ResNet-50 model.

D.2 Forgetting a class

Experiment details. In Section 5.2, we use COAR-EDIT to selectively forget a class of a ResNet-50 model on ImageNet. In this experiment, we set the “target” examples to be set of 10 examples from the class to be forgotten and the “reference” examples to be a set of 50 randomly selected ImageNet examples. Using these examples, we use COAR-EDIT to ablate components (9) that decrease the average correct-class margin (5) of the target examples without impacting the average margin over the reference examples.

Additional experiments We show that COAR-EDIT can be used to selectively forget additional ImageNet classes. Specifically, in Figure 23, we reproduce the COAR-EDIT experiment in Section 5.2 on three additional ImageNet classes: “folding chair”, “military uniform”, and “revolver”.

Like in Figure 4, we again observe that COAR-EDIT can specifically degrade the accuracy on the target class without impacting the average accuracy over the train or test set by ablating a few components (convolution filters) in the ResNet-50 model.

D.3 Improving subpopulation robustness.

Experiment details. In Section 5.3, we use COAR-EDIT to improve subpopulation robustness of models trained on two benchmark datasets: Waterbirds and CelebA. In both cases, we fine-tune an ResNet-50 model via standard “empirical risk minimization” using SGD hyperparameters taken from Sagawa et al. [SKH+20]. The resulting fine-tuned models attain 64% and 47% worst-subpopulation accuracy on the Waterbirds and CelebA test sets, respectively. To improve subpopulation robustness on Waterbirds, we set the “target” examples to a set of 10 random training examples from the “waterbirds on land” (the worst-performing subpopulation) and the “reference” examples to be 10 random examples from other subpopulations. Analogously, for CelebA, we set the “target” examples to the set of 20 random examples from the “blond male” worst-performing subpopulation and the “reference” examples to 20 random examples from other subpopulations. Then, we use COAR-EDIT to identify components that, when ablated, increase the average correct-class margin (5) of the target examples without impacting the average margin over the reference examples. In both cases, the number of components to ablate is a hyperparameter that we select by tracking the worst-subpopulation accuracy on a validation set.

D.4 Mitigating backdoor attacks.

Experiment details. We now describe the experiment setup in Section 5.4, where we used COAR-EDIT to mitigate the effect of a backdoor attack on a ResNet-18 model trained on a backdoored CIFAR-10 dataset. The CIFAR-10 dataset is modified by adding a small blue-squared trigger to the upper left corner of 50% of examples in the “airplane” class. Training a model with standard SGD hyperparameter on this dataset causes the model to spuriously associate the trigger with the “airplane” class, leading to a backdoor attack. That is, while the resulting model attains 89% test accuracy, applying the attack to examples in the test set causes the model to misclassify them as “airplanes”, resulting in 37% accuracy on test examples with the trigger. To mitigate the effect of the backdoor attack, we first sample ten examples from the training set. Then, we set the “target” examples to these two examples *with* the trigger and the “reference” examples to these two examples *without* the trigger. Then, we use COAR-EDIT to ablate components (9) that increase the correct-class margin (5) of the target examples without impacting the average margin over the reference examples.

Additional analysis. Recall that our experiment in Section 5.4 shows that COAR-EDIT can significantly mitigate the effect of a backdoor attack on a ResNet-18 model by ablating a few backdoor-specific components. We now qualitatively analyze the components ablated via COAR-EDIT to mitigate the effect of a backdoor attack in Figure 24. Specifically, we visualize the ablated components (convolution filters in this case) using the input-times-gradient saliency map method from the Captum library [KMM+20]. As shown in Figure 24, these visualizations suggest that the ablated components are sensitive to the blue-squared trigger.

D.5 Improving robustness to typographic attacks.

Experiment details. In Section 5.5 and Figure 7 in particular, we show that COAR-EDIT can be used to improve robustness of zero-shot CLIP classifiers to typographic attacks. In this experiment, we consider a zero-shot CLIP ViT-B/16 classifier [RKH+21] and specify a computation graph over 82,944 components, where each component corresponds to a weight vector in the ViT (across all layers). We evaluate the robustness of this model in a zero-shot setting on 180 images and four real-world typographic attacks—“taxi”, “twitter”, “EU”, and “iPad”—taken from the dataset in [MTB22]. We also consider synthetic typographic attacks, where we render a blob of text on a white background and place it in the center of a given image. The zero-shot performance of the CLIP model drops from 95% to 51% and 54% on the real and synthetic typographic attacks, respectively. To improve robustness, we set the “target” examples to be the 25 examples *with* a randomly picked synthetic attack and the “reference” examples to the same set of examples *without* any attack. Then, we use COAR-EDIT to ablate components (9) that increase the average correct-class margin (5) of the target examples without impacting the average margin over the reference examples. We use a validation set comprising examples with and without the synthetic attack to select the number of components to ablate from the model.

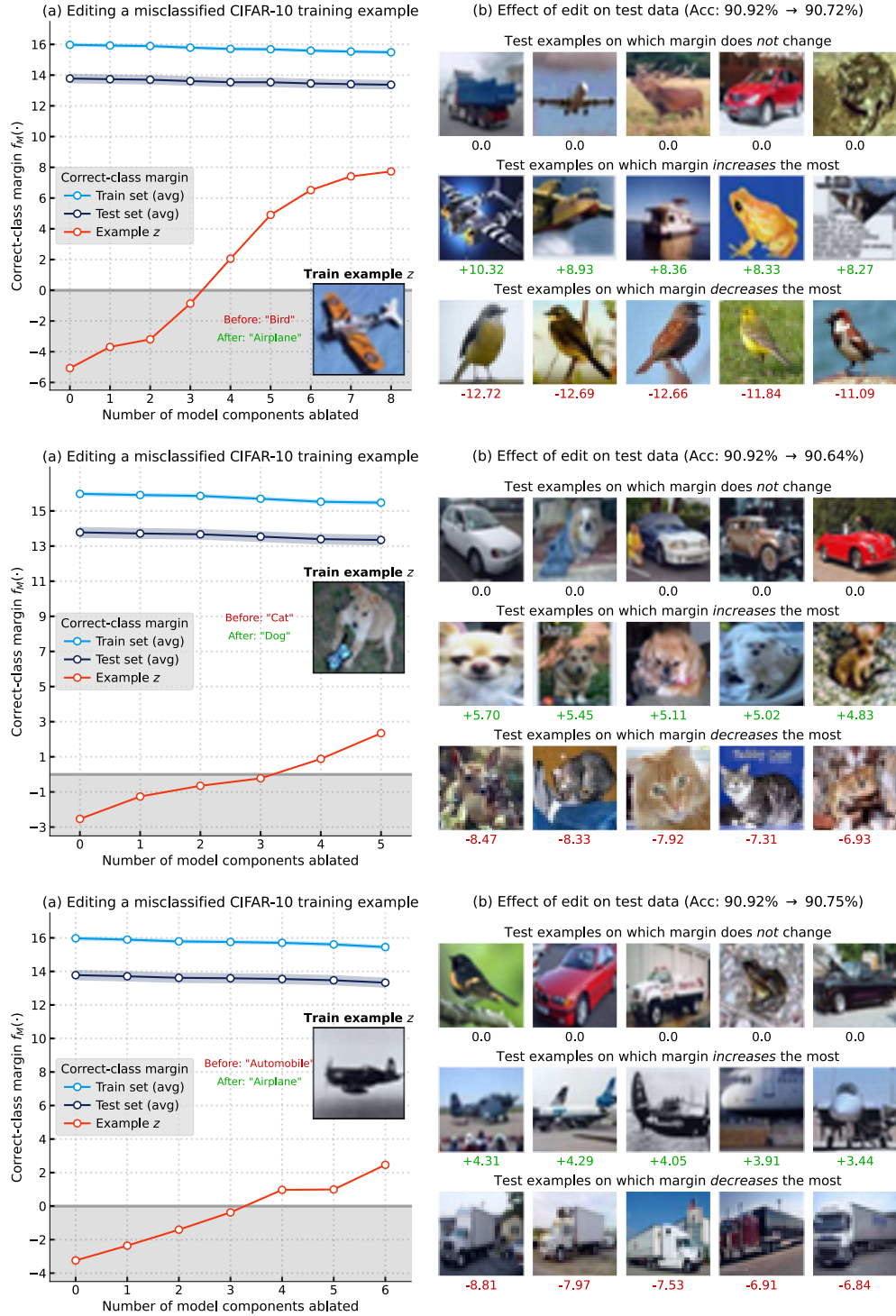


Figure 19: **Correcting misclassified CIFAR-10 examples via COAR-EDIT.** We reproduce the COAR-EDIT experiment from Section 5.1 on the CIFAR-10 dataset. Specifically, each row corresponds to CIFAR-10 test example that is misclassified by a ResNet-18 model. The left subplot in each row shows how applying COAR-EDIT (by ablating components (9)) increases the correct-class margin (5) of the misclassified example without impacting the average margin over the train or test set. The right subplot reports the drop in overall test accuracy and visualizes examples with correct-class margins that change the most or least due to the edit.

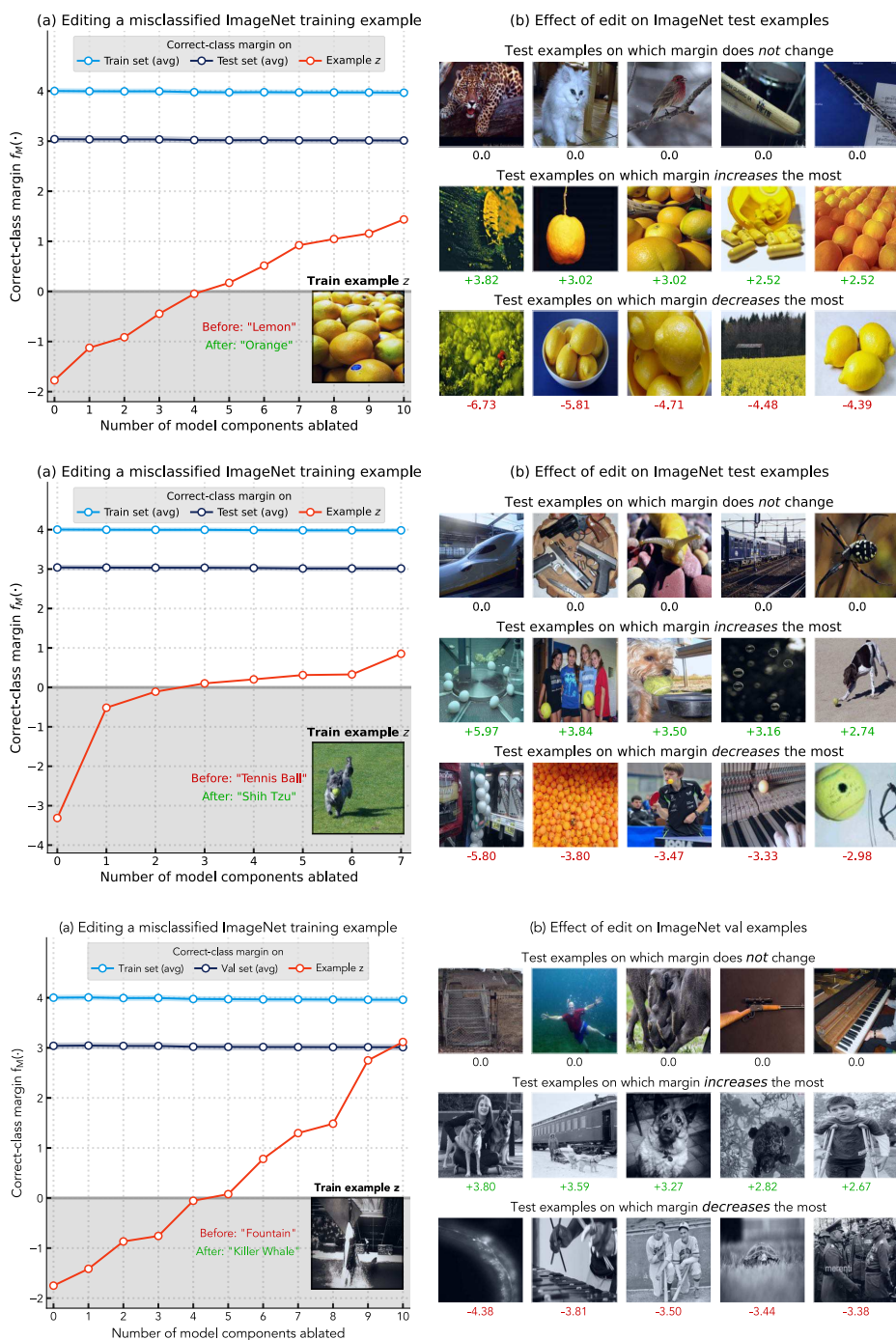


Figure 20: **Correcting misclassified ImageNet examples via COAR-EDIT.** We reproduce the COAR-EDIT experiment from Section 5.1 on additional ImageNet examples (one per row) misclassified by a ResNet-50 model. The left subplot shows that applying COAR-EDIT (by ablating components (9)) increases the correct-class margin (5) of the misclassified example without impacting the average margin over the train or test set. (Right) The right subplot visualizes examples with margins that change the most or least due to the edit.

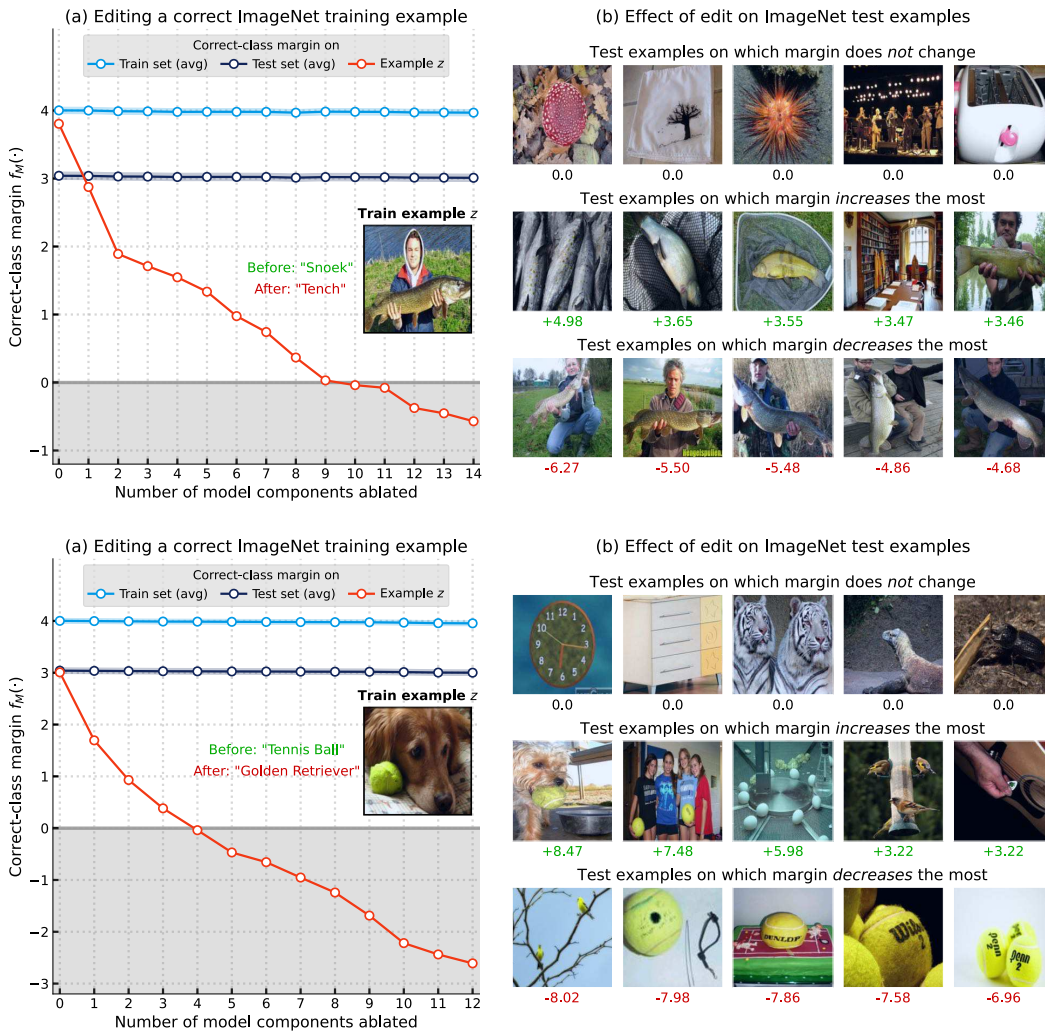


Figure 21: **Adversarially inducing misclassifications on ImageNet examples via COAR-EDIT.** Each row corresponds to an ImageNet test example that is correctly classified by a ResNet-50 model. In the left subplot of each row, we show that applying COAR-EDIT (by ablating the top- k components (9)) decreases the correct-class margin (5) of the correctly classified example without impacting the average margin over the train or test set. On the right, we show that the edit does not impact visually dissimilar examples, but does increase or decrease the correct-class margin of examples containing visually similar objects, e.g., tennis balls in the second row.

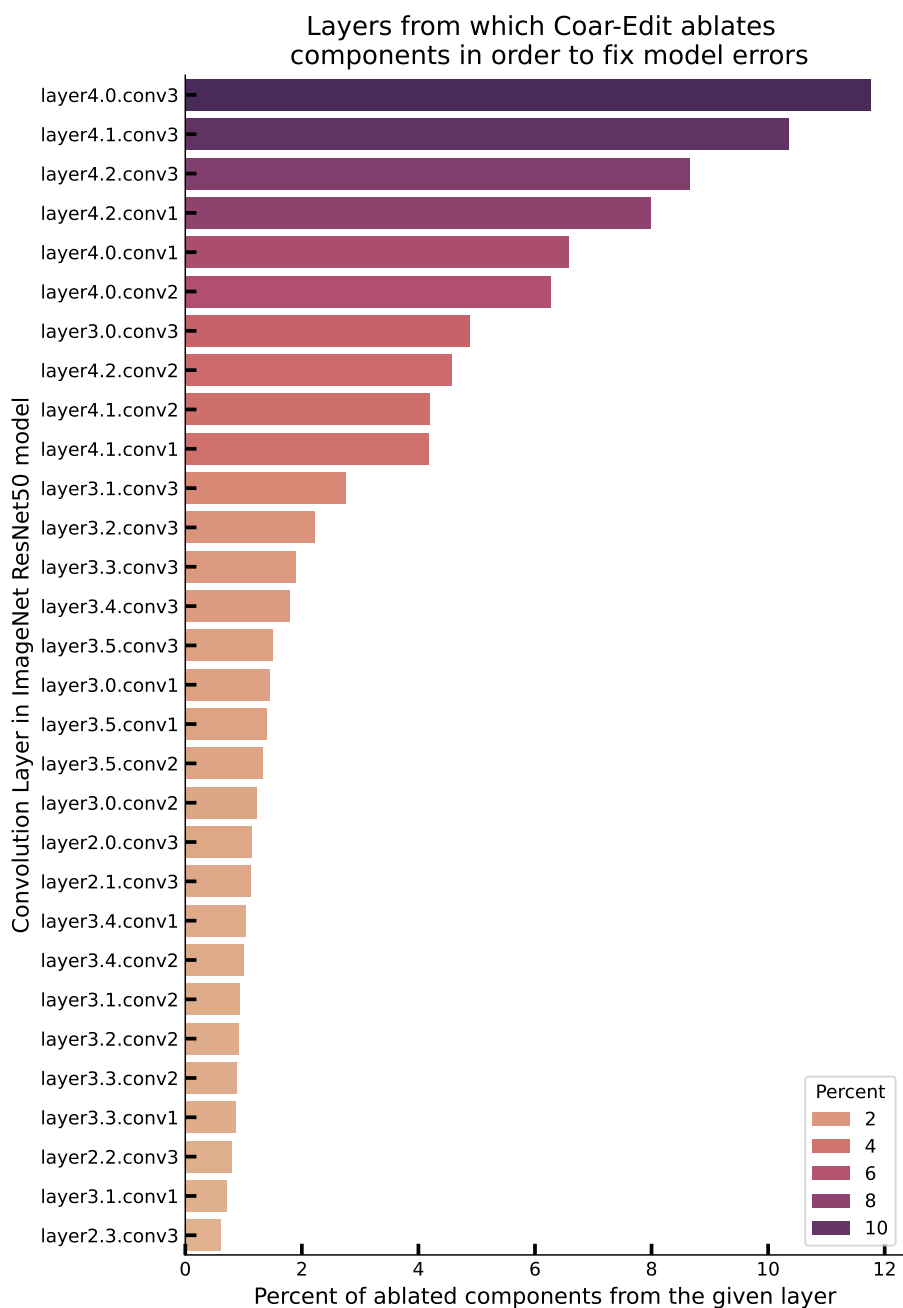


Figure 22: **Which components does COAR-EDIT target to fix model errors?** We analyze the specific convolution layers from which COAR-EDIT ablates components (convolution filters) to correct ImageNet examples misclassified by a ResNet-50 model. On the y -axis, we plot the 30 most common convolution layers corresponding to the ablated components. On the x -axis, we plot the percentage of ablated components that belong to each convolution layer. We find that COAR-EDIT primarily targets convolution filters from the last few layers (closest to the output) of the ResNet-50 model in order to make fine-grained edits that do not impact overall model performance. For example, more than 25% of the ablated components belong to `layer4.{0,1,2}.conv3`—the last convolution layer in the first three residual blocks of the last layer group of the ResNet-50 model.

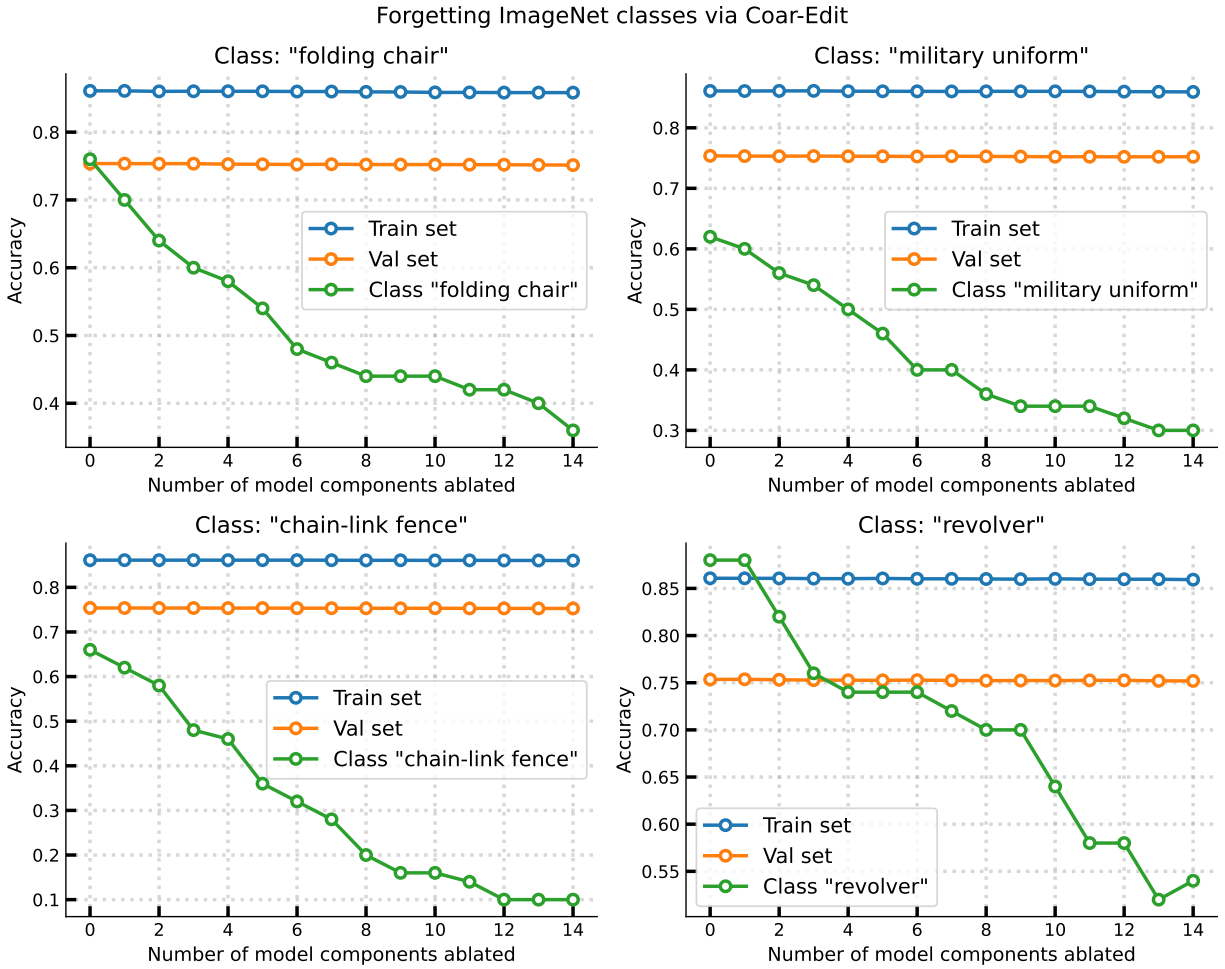


Figure 23: **Forgetting ImageNet classes via COAR-EDIT.** We reproduce the COAR-EDIT experiment from Section 5.2 on additional ImageNet classes (one per subplot). Specifically, in each subplot, we find that ablating 15 of 22,720 convolution filters (identified via COAR-EDIT) suffices to significantly degrade the accuracy of a ResNet-50 model on a specific class (in green). This edit is targeted in that it does not impact the average accuracy over the train set (in blue) or test set (in orange).

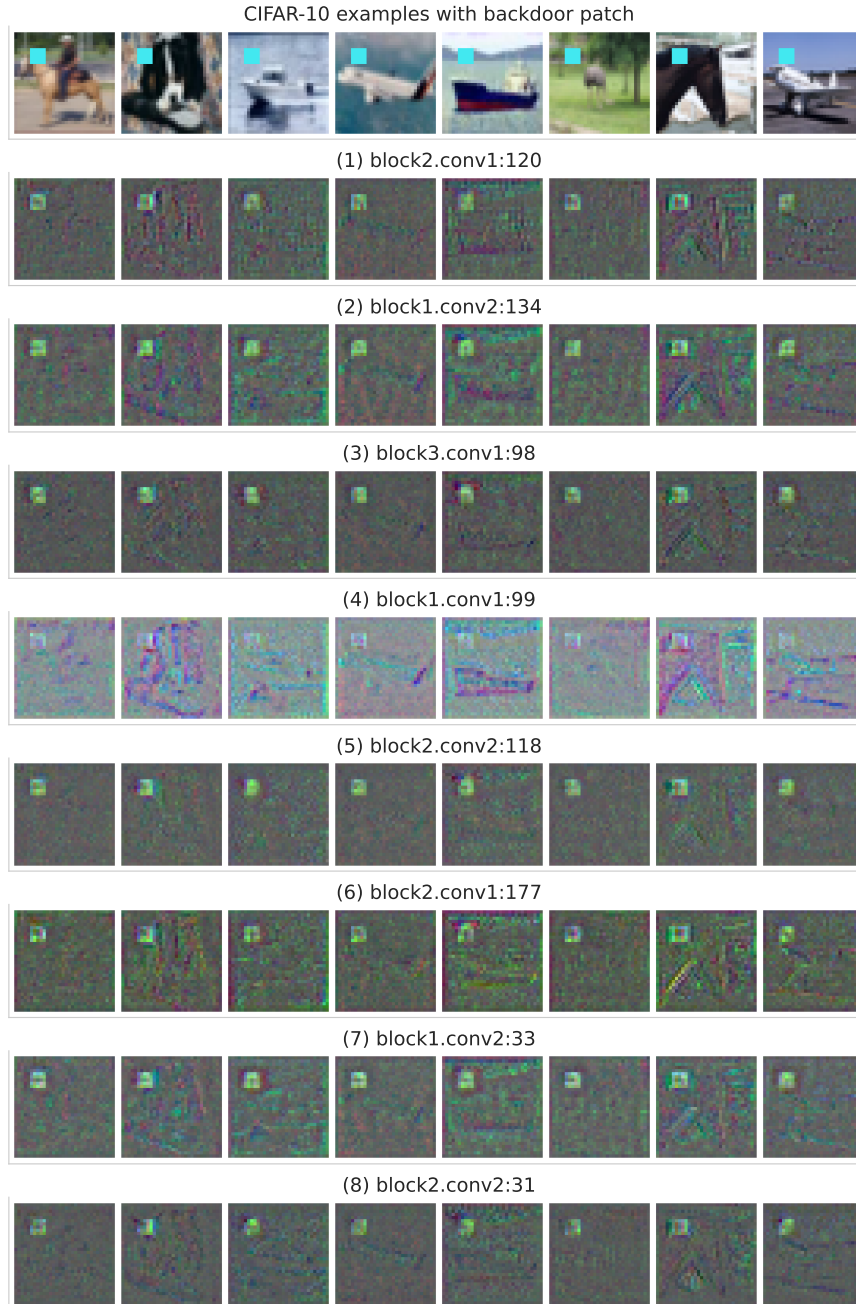


Figure 24: **Visualizing components ablated via COAR-EDIT to mitigate a backdoor attack.** Recall that in Section 5.4, we used COAR-EDIT to mitigate the effect of a backdoor attack (a blue-squared spurious trigger) on a ResNet-18 model trained on a backdoored CIFAR-10 dataset. Here, we visualize the components ablated via COAR-EDIT to reduce the model’s reliance on this spurious feature. The first row shows a set of random examples from the modified CIFAR-10 test set that contain the trigger. Each subsequent row corresponds to an ablated component—a convolution filter of the ResNet-18 model in this case. In each of these rows, we use the input-times-gradient saliency map method from the Captum library [KMM+20] to (qualitatively) highlight parts of the examples that are most “important” for the ablated component’s output. These maps suggest that all ablated components are sensitive to the blue-squared trigger.

E Analyzing design choices in COAR

In this section, we analyze three design choices in COAR: (a) the train-time ablation fraction α used to sample a subset of components $C' \subset C$ of size $\alpha|C|$, (b) the ablation method (Remark 2) used to intervene on the sampled components C' , and (c) the specific model output function used to compute component counterfactuals $f_M(\cdot, C')$ (1), i.e., model output $f_M(\cdot)$ after ablating the component subset C' .

E.1 Effect of ablation fraction

The first step of COAR—constructing a component dataset (Equation 2)—requires choosing an ablation fraction $\alpha \in (0, 1)$. This hyperparameter determines the size of the random α -fraction subsets $C' \subset C$ used to compute component counterfactuals. A priori, however, it is not clear which ablation fraction α is best suited for learning accurate component attributions. For example, ablating too large a component subset (large α) can induce a significant drop in model performance to a point where the ablated model is no longer representative of the original model.

Effect of train-time ablation fraction α_{train} We use two metrics to quantify the effect of ablation fraction α on model outputs:

- **Change in model performance.** We measure the effect of ablating random α -fraction subsets $C' \subset C$ of components on model performance, e.g., test accuracy.
- **Correlation between example-level model outputs.** We measure the correlation between model outputs before and after ablation, e.g., logits or margins.

We use these (heuristic) metrics to ensure that the ablations are not too severe to nullify model performance and that the outputs of the ablated models are still predictive of the outputs of the original model.

Effect of train-time ablation fraction α_{train} . Figure 25 evaluates how varying the train-time ablation fraction α_{train} changes both metrics—model performance and correlation between model outputs—for all three settings considered in Section 4: CIFAR-10 ResNet-18, ImageNet ResNet-50, and ImageNet ViT-B/16. In all three settings, we find that model accuracy and margin correlation decrease as the ablation fraction α increases. For instance, ablating 15% of components ($\alpha = 0.15$) results in a significant accuracy drop for ResNets, but not for ViTs. On the other hand, ablating 1% of all components ($\alpha = 0.01$) results in a small drop in accuracy and correlation, e.g., for the ResNet-18 model trained on CIFAR-10 (first row of Figure 25). Therefore, our experiments in Section 4 use $\alpha = 0.10$ for the CIFAR-10 model and $\alpha = 0.05$ for both ImageNet models. These findings also suggest that the choice of α depends on the model architecture and the task at hand, e.g., ViTs are more robust to zero ablations than ResNets.

E.2 Effect of ablation method

As discussed in Remark 2, we use a simple ablation method that sets the weights/activations of a subset of components $C' \subset C$ to zero. However, our method COAR is not dependent on any specific ablation method, and can be used to compute component attributions with other ablation methods as well.

Alternative ablation method based on scaling. In this section, we consider an alternative ablation method that scales down the activations of a component by a factor of $\gamma \in [0, 1]$. Note that setting $\gamma = 0$ corresponds to the zero ablation method described in Remark 2; we use $\gamma = 0.5$ in our experiments.

Experiment results. We find that the alternative scaling-based ablation maintains high correlation between model outputs before and after ablations, resulting in accurate component attributions. Specifically, we make three key observations.

- We first observe that on a ResNet-18 model trained on CIFAR-10, the scaling-based ablation method described above maintains high correlation between model outputs before and after ablation, even at high ablation fractions $\alpha \in \{0.30, \dots, 0.05\}$ (fourth row of Figure 25).
- Then, in Figure 26, we apply COAR with the scaling-based ablation method to a CIFAR-10 ResNet-18 model. The resulting component attributions attain an average correlation of more than 0.75 for most ablation fractions $\alpha \in \{0.40, \dots, 0.01\}$. The correlation between COAR attribution estimates and ground-truth counterfactuals is high across a range of ablation fractions α from 0.01 to 0.45.
- In Figure 27, we compare COAR attributions computed with the scaling ablations to attributions computed with zero-ablations. We find that (a) these attributions exhibit high cosine similarity (Figure 27a) and that (b) attributions learned with scaling-based ablations are predictive of ground-truth component counterfactuals computed using zero-ablations (Figure 27b). This indicates that both ablations—scaling down the activations of a component by a factor of $\gamma = 0.5$ and setting the activations of a component to zero—change model outputs in a similar manner.

E.3 Effect of model output function

Recall that in Section 4, we use the correct-class margin (5) as the model output function to estimate COAR attributions for classification tasks. However, our approach is not tied to a specific model output function. Depending on the task at hand, one can use an alternative model output function to estimate COAR attributions. For example, in a multi-label classification task, we can also use the logit of a fixed class of interest as the model output function to estimate COAR attributions. In Figure 12, we apply COAR to a pre-trained ImageNet ResNet50 model fine-tuned on MIMIC-CXR [JPG+19]—a dataset of labeled chest radiographs—and set the model output function to be the logit of the “Cardiomegaly” class. Our results show that COAR attributions remain predictive with this model output function, and attain a correlation of 0.7 and 0.6 with the ground-truth counterfactuals on “Cardiomegaly” logits when $\alpha = \alpha_{\text{train}} = 0.05$ and $\alpha = 0.10$ respectively. Additionally, in Appendix B, we also apply COAR to the next-token prediction task in language modeling, using average correct-class margin over all tokens in a given sequence as the model output function.

Effect of ablation fraction on model outputs

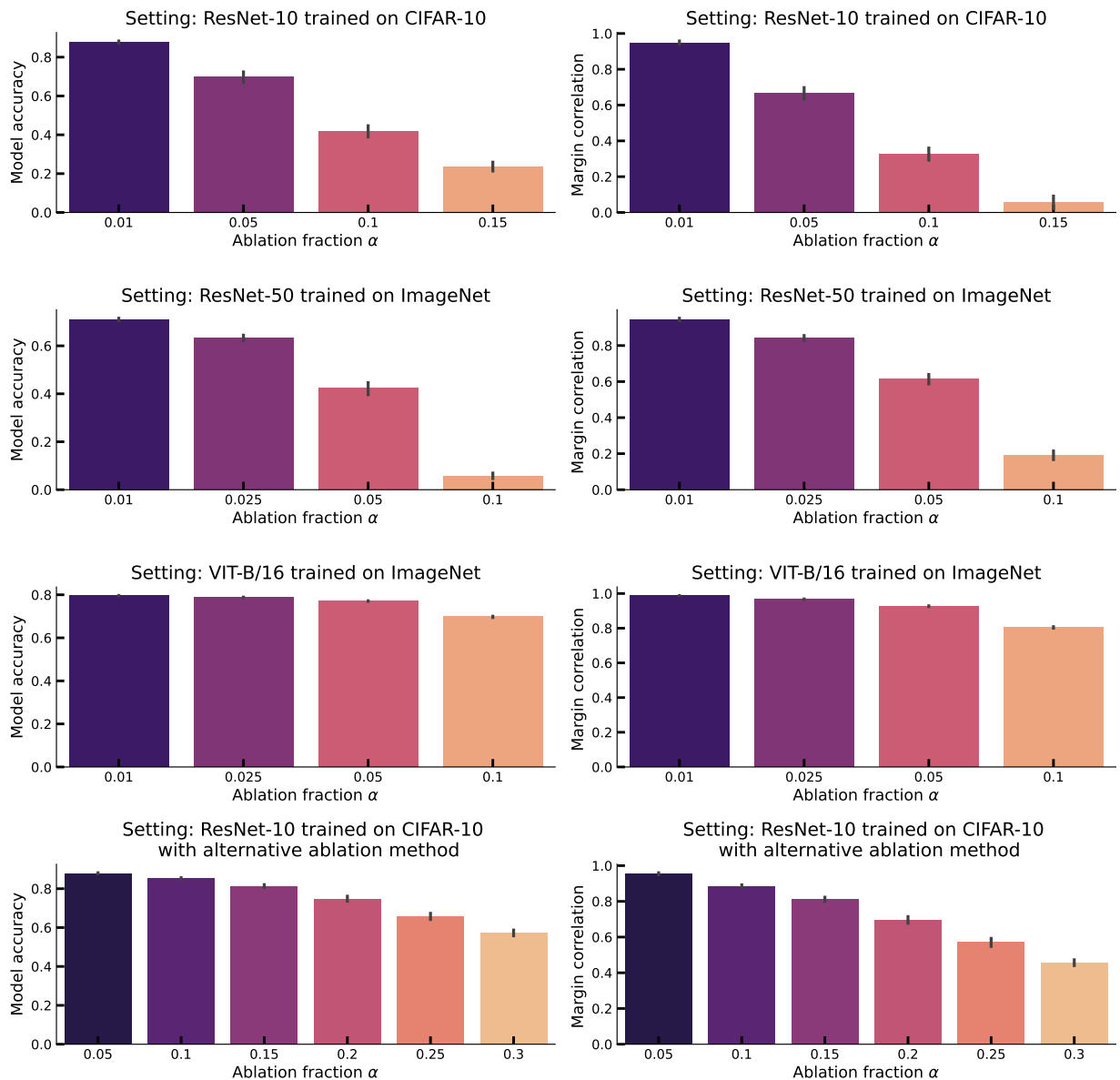


Figure 25: **Effect of ablation fraction α on model outputs.** We evaluate the effect of ablating α -fraction subsets $C' \subset C$ of components (x -axis) on model accuracy (y -axis in the left column) and the correlation between model outputs before and after ablation (y -axis in the right column). In all settings considered in Section 4 (one per row), we find that model accuracy and margin correlation gradually decrease as the ablation fraction α increases. See Appendix E.1 for more details.

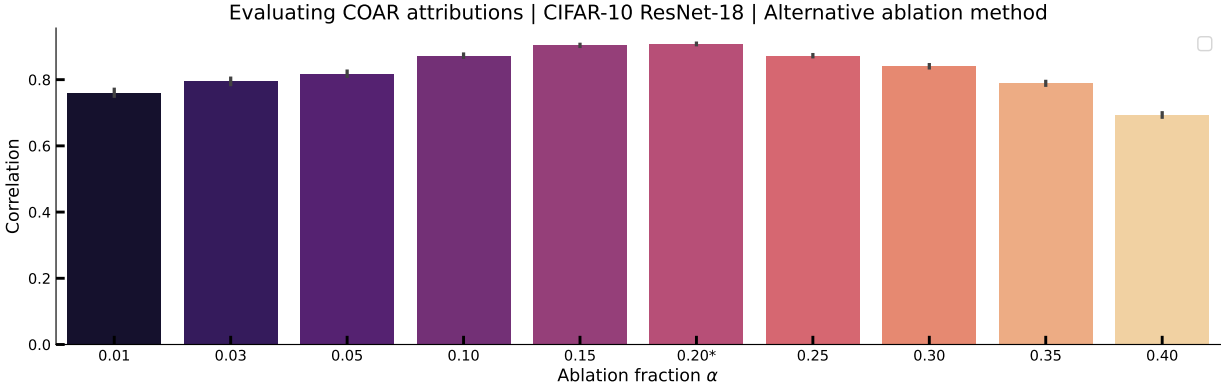


Figure 26: **Effect of ablation method on COAR attributions.** We estimate COAR attributions for a CIFAR-10 ResNet-18 model using an alternative ablation method that scales down the activations of a subset of components $C' \subset C$ by a factor of γ (0.5 in this case) instead of setting them to zero. The resulting attribution-derived estimates (4) exhibit high correlation (y -axis) with ground-truth component counterfactuals. See Appendix E.2 for more details.

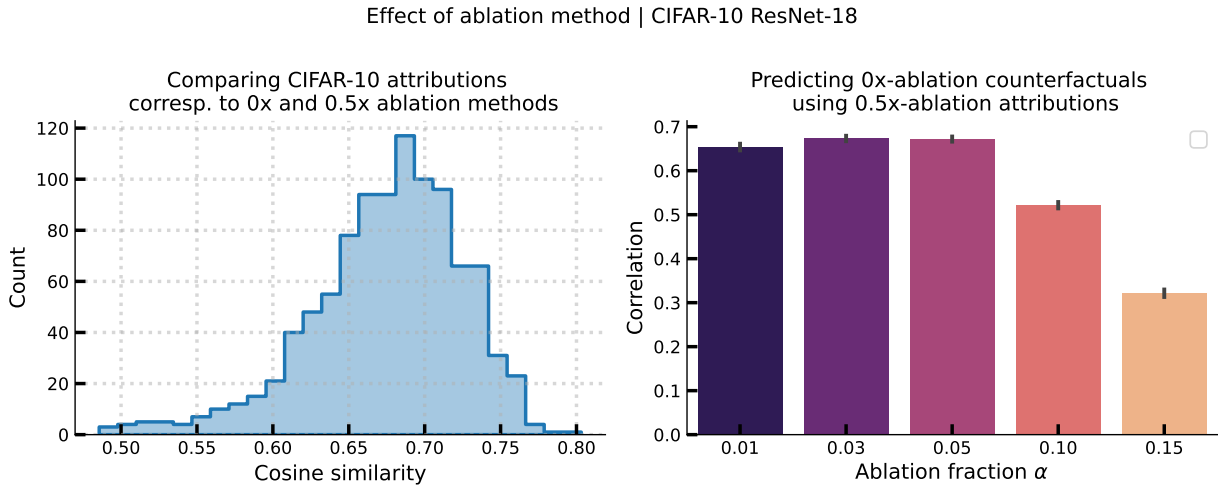


Figure 27: **Comparing COAR attributions estimated with different ablation methods.** We compare COAR attributions on a CIFAR-10 ResNet18 model computed with the zero-ablation method Remark 2 to attributions computed with the alternative ablation method described in Appendix E.2. The left plot shows that the paired attributions (corresponding to each example) exhibit high cosine similarity. The right plot shows that the counterfactual estimates (4) computed using attributions from the alternative ablation method are predictive of ground-truth component counterfactuals computed using the zero ablation method. See Appendix E.2 for more details.

